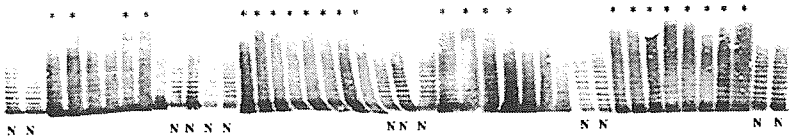

Figure 6. Analysis of VWF multimers of patients with sepsis-induced DIC. VWF multimers in the plasma of patients with sepsis-induced DIC with ADAMTS13 activity levels lower than 20% were analyzed by SDS-agarose gel electrophoresis, as described in "Patients, materials, and methods." VWF multimer patterns of patients and healthy subjects (N) were analyzed simultaneously. *Representative unusually large multimers of VWF found in the plasma of patients with ADAMTS13 activity levels lower than 20%.

unusually large VWF multimers in humans. TTP is a fatal thrombotic microangiopathic disease if patients are not treated appropriately, but the incidence of TTP is low.[8,22] While searching for the role of ADAMTS13 in common thromboembolic diseases, we found severe secondary ADAMTS13 deficiency in patients with sepsis-induced DIC and showed its clinical correlation to the development of renal failure in this study.

DIC is associated with a variety of disease states such as sepsis, advanced malignancy, severe tissue damage, and pregnancy-related complications. Sepsis may be the most common pathogenic disease that leads to the development of DIC, and the endotoxemia and high cytokine levels in the circulation are thought to induce tissue factor expression that in turn initiates fibrin thrombus formation in the circulation. Microthrombi formed in the circulation cause ischemia of and damage to a variety of organs. Lines of evidence have suggested that proteases released from white blood cells may also be involved in the development of organ injuries. This study showed that patients with sepsis-induced DIC frequently exhibited decreased antigen and activity levels of ADAMTS13 and that severe ADAMTS13 deficiency was found in these patients at high incidence. Many patients in this study had undergone transfusion with ADAMTS13-containing blood products, such as fresh frozen plasma and platelet concentrates, soon before blood sample collection for the determination of ADAMTS13 levels, suggesting that the levels of ADAMTS13 in the plasma samples of these patients might not reflect the severity of ADAMTS13 deficiency before blood transfusion. Thus, severe secondary ADAMTS13 deficiency in sepsis-induced DIC might be more common. Clinical manifestations and laboratory data of these patients with sepsis and secondary severe ADAMTS13 deficiency were nearly indistinguishable from those of patients with TTP, though the former had evidence of infection (Table 2), indicating that there exists a subset of patients who have secondary severe ADAMTS13 deficiency caused by sepsis and in whom the disease course is clinically similar to that of TTP. In addition, they might also have the same ADAMTS13 deficiency pathophysiology for the development of TMA seen in patients with idiopathic TTP.

Organ failure might be caused by tissue factor–dependent fibrin thrombus formation and platelet aggregation because of severe ADAMTS13 deficiency in the patients with sepsis-induced DIC with ADAMTS13 activity levels lower than 20%. This notion was supported by the correlation between severe secondary ADAMTS13 deficiency and renal failure in patients with sepsis-induced DIC with ADAMTS13 activity levels lower than 20%. We could not find any significant difference in the ADAMTS13-specific activity levels between these 2 groups (not shown). One possibility is that small molecular forms of ADAMTS13 could be lost in urine because of renal injuries. However, we could not determine whether this was the case because no urine samples were available for study.

In a previous report by Reife et al,[25] patients with TMA who did not have DIC were analyzed for the correlation between ADAMTS13 activity levels and serum creatinine levels without distinguishing TTP from HUS. They found that creatinine levels in patients with severely decreased ADAMTS13 activity levels were significantly lower than those in patients without severely decreased ADAMTS13 activity levels. These data are contrary to our findings that patients with severe ADAMTS13 deficiency (ADAMTS13 activity less than 20%) had significantly higher serum creatinine levels than did patients with the ADAMTS13 activity levels higher than 20%. Given that patients with HUS were not distinguished from patients with TTP in the report by Reife et al,[25] it is possible that the patients without severe ADAMTS13 deficiency in that study included patients with HUS. We studied patients with sepsis-induced DIC, and this difference in patient groups explains the opposing findings. There was no apparent difference between the platelet counts of patients with ADAMTS13 activity levels less than 20% and those of patients with ADAMTS13 activity levels greater than 20%. The combination of underlying DIC and platelet transfusion in these patients may account for the data.

The presence of the unusually large multimers of VWF in the plasma of patients with severe secondary ADAMTS13 deficiency and its correlation with serum creatinine levels supports the notion that severe secondary ADAMTS13 deficiency may correlate with the development of renal failure in sepsis-induced DIC. There was no significant correlation between the unusually large multimers of VWF and ADAMTS13 activity levels, possibly because of technical difficulties in determining the unusually large VWF multimers and the differences in endothelial cell damage among these patients.

Decreased specific activity of ADAMTS13, presumably caused by its cleavage by proteases, was a mechanism for severe secondary ADAMTS13 deficiency in patients with sepsis-induced DIC. Various proteases have been shown to degrade ADAMTS13 in vitro.[21] Thrombin and plasmin are generated in DIC, and these enzymes may cleave ADAMTS13, resulting in the inactivation of ADAMTS13. Our data suggest that granulocyte elastase may be one of the proteases that cleave ADAMTS13, together with thrombin and plasmin, under in vivo pathologic conditions. In this regard, the case report by Galbusera et al[26] of chronically relapsing

Table 4. Correlation between presence of unusually large multimers of VWF and serum creatinine levels of patients with sepsis-induced DIC and ADAMTS13 activity levels lower than 20%

	Presence, n = 26	Absence, n = 25	P
Creatinine, mg/dL	2.39 ± 2.24	1.34 ± 1.35	< .05*
ADAMTS13 activity, %	6.6 ± 6.8	8.9 ± 6.0	NS

Values are mean ± SD.

To convert creatinine from milligrams per deciliter to micromoles per liter, multiply milligrams per deciliter by 88.4.

Presence indicates unusually large VWF multimers present in the plasma of patients; absence, unusually large VWF multimers absent in the plasma of patients. NS, not significant.

*Statistically significant (Welch *t* test).

TTP—which showed that α1-antitrypsin (the physiologic granulocyte elastase inhibitor) therapy was effective at preventing the appearance of unusually large VWF multimers in the circulation but not at preventing TTP relapse—was interesting and suggested the link between granulocyte elastase and cleavage of ADAMTS13. Correlation between ADAMTS13 activity and antigen levels and E-XDP levels, not only in patients with TTP but also in patients with pathogenic *E coli* infection–related HUS, would be a further study to investigate the role of granulocyte elastase in TMA development. Specific inhibitors of these proteases are present at high concentrations in blood, indicating that cleavage of ADAMTS13 by these proteases may depend on the kinetic balance between ADAMTS13, the proteases, and their inhibitors. Thus, cleavage of ADAMTS13 by these proteases may not proceed completely in vivo. It is possible that other proteases could also digest ADAMTS13 in the disease state. This possibility should be investigated in a future study.

Because serum albumin levels decreased in most patients, liver injuries associated with the underlying disease might be an additional mechanism for decreasing ADAMTS13 antigen levels given that this enzyme is synthesized in the liver. Mutations or polymorphisms of the *ADAMTS13* gene are another possible cause of a decrease or an increase of ADAMTS13-specific activity. These possibilities should also be explored in future studies.

In conclusion, the precise analysis of ADAMTS13 antigen and activity levels in disease states offers insight into the roles of ADAMTS13 in thromboembolic diseases. Severe ADAMTS13 deficiency takes place secondarily in disease states such as sepsis-induced DIC, and it may not be specific for idiopathic TTP and may not have a solo diagnostic value for idiopathic TTP. Although the mechanisms of severe ADAMTS13 deficiency in sepsis are different from those of idiopathic TTP, the clinical features of patients with sepsis-induced DIC and severe ADAMTS13 deficiency are similar to those of patients with idiopathic TTP. Sepsis may have the same pathophysiology of severe ADAMTS13 deficiency for TMA development as idiopathic TTP, raising the possibility of novel supportive therapies for patients with sepsis and severe ADAMTS13 deficiency, such as ADAMTS13 supplementation, α1-antitrypsin administration, and use of synthetic granulocyte elastase inhibitors. Given that severe secondary ADAMTS13 deficiency might correlate with the development of organ injury in patients with sepsis-induced DIC, determining the ADAMTS13 levels of patients in severe condition at the time of hospital admission would provide better understanding of the extent of disease. Current analyses of ADAMTS13 levels in disease states are retrospective; thus, prospective study is needed for the timely execution of ADAMTS13 supplementation for patients not only with TTP but also with secondary ADAMTS13 deficiency.

References

1. Gerritsen HE, Robles R, Lämmle B, Furlan M. Partial amino acid sequence of purified von Willebrand factor-cleaving protease. Blood. 2001;98: 1654-1661.
2. Fujikawa K, Suzuki H, McMullen B, Chung D. Purification of human von Willebrand factor-cleaving protease and its identification as a new member of metalloprotease family. Blood. 2001;98:1662-1666.
3. Levy GG, Nichols WC, Lian EC, et al. Mutation in a member of ADAMTS gene family cause thrombotic thrombocytopenic purpura. Nature. 2001;413:488-494.
4. Zheng X, Chung D, Takayama TK, Majerus EM, Sadler JE, Fujikawa K. Structure of von Willebrand factor-cleaving protease (ADAMTS-13), a metalloprotease involved in thrombotic thrombocytopenic purpura. J Biol Chem. 2001;276: 41059-41063.
5. Soejima K, Mimura N, Hirashima M, et al. A novel human metalloprotease synthesized in the liver and secreted into the blood: possibly, the von Willebrand factor-cleaving protease? J Biochem (Tokyo). 2001;130:475-480.
6. Moake JL Thrombotic microangiopathies. N Engl J Med. 2002;347:589-600.
7. Furlan M, Robles R, Lamie B. Partial purification and characterization of a protease from human plasma cleaving von Willebrand factor to fragments produced by in vivo proteolysis. Blood. 1996;87:4223-4234.
8. Furlan M, Robles R, Galbusera M, et al. Von Willebrand factor-cleaving protease in thrombotic thrombocytopenic purpura and the hemolytic uremic syndrome. N Engl J Med. 1998;339:1578-1584.
9. Tsai HM, Lian EC. Antibodies to von Willebrand factor-cleaving protease in acute thrombotic thrombocytopenic purpura. N Engl J Med. 1998; 339:1585-1594.
10. Loof AH van Vliet HH, Kappers-Klunne MC. Low activity of von Willebrand factor-cleaving protease is not restricted to patients suffering from thrombotic thrombocytopenic purpura. Br J Haematol. 2001;112:1087-1088.
11. Veyradier A, Brivet F, Wolf M, et al. Total deficiency of specific von Willebrand factor-cleaving protease and recovery following plasma therapy in one patient with hemolytic-uremic syndrome. Hematol J. 2001;2:352-354.
12. Remuzzi G, Galbusera M, Noris M, et al. von Willebrand factor cleaving protease (ADAMTS-13) is deficient in recurrent and familial thrombotic thrombocytopenic purpura and hemolytic uremic syndrome. Blood. 2002;100:778-785.
13. Studt JD, Bohm M, Budde U, Girma JP, Varadi K, Lämmle B. Measurement of von Willebrand factor-cleaving protease (ADAMTS-13) activity in plasma: a multicenter comparison of different assay. J Thromb Haemost. 2003;1:1882-1887
14. Kokame K, Matsumoto M, Soejima K, et al. Mutations and common polymorphisms in ADAMTS13 gene responsible for von Willebrand factor-cleaving protease activity. Proc Natl Acad Sci U S A. 2002;99:11902-11907
15. Gando S, Kameue T, Morimoto Y, Matsuda N, Hayakawa M, Kemmotsu O. Tissue factor production not balanced by tissue factor pathway inhibitor in sepsis promotes poor prognosis. Crit Care Med. 2002;30:1729-1734
16. American College of Chest Physicians/Society of Critical Care Medicine Consensus Conference: Definitions for sepsis and multiple organ failure and guidelines for the use of innovative therapies in sepsis. Crit Care Med. 1992;20:864-874.
17. Kohler G, Milstein C. Continuous cultures of fused cells secreting antibody of predefined specificity. Nature 1975;256:495-497.
18. Soejima K, Matsumoto M, Kokame K, et al. ADAMTS-13 cysteine-rich/spacer domains are functionally essential for von Willebrand factor cleavage. Blood. 2003;102:3232-3237.
19. Ono T, Sogabe M, Ogura M, Furusaki F. Automated latex photometric immunoassay for total plasminogen activator inhibitor-1 in plasma. Clin Chem. 2003;49:987-989.
20. Kohno I, Inuzuka K, Itoh Y, et al. A monoclonal antibody specific to the granulocyte-derived elastase-fragment D species of human fibrinogen and fibrin: its application to the measurement of granulocyte-derived elastase digests in plasma. Blood. 2000;95:1721-1728.
21. Crawley JT, Lam JK, Rance JB, Mollica LR, O'Donnell JS, Lane DA. Proteolytic inactivation of ADAMTS13 by thrombin and plasmin. Blood. 2005;105:1085-1093.
22. Bianchi V, Robles R, Alberio L, Furlan M, Lammle B. von Willebrand factor cleaving protease (ADAMTS-13): in thrombocytopenic disorders: a severely deficient activity is specific for thrombotic thrombocytopenic purpura. Blood. 2002; 100:710-713.
23. Mannucci PM, Canciani MT, Forza I, Lussana F, Lattuada A, Rossi E. Change in health and disease of the metalloprotease that cleaves von Willebrand factor. Blood. 2001;98:2730-2735.
24. Dong J, Moake JL, Nolasco L, et al. ADAMTS-13 rapidly cleaves newly secreted ultralarge von Willebrand factor multimers on the endothelial surface under flowing conditions. Blood. 2002;100: 4033-4039.
25. Raife T, Atkinson B, Montgomery R, Vesely S, Friedman K. Severe deficiency of VWF-cleaving protease (ADAMTS13) activity defines a distinct population of thrombotic microangiopathy patients. Transfusion. 2004;44:146-150.
26. Galbusera M, Ruggenenti P, Noris M, et al. α1-Antitrypsin therapy in a case of thrombotic thrombocytopenic purpura. Lancet. 1995;345:224-225.

Protection of Plasminogen Activator Inhibitor-1-Deficient Mice from Nasal Allergy[1]

Takayuki Sejima,*† Seiji Madoiwa,† Jun Mimuro,† Teruko Sugo,† Kiyotaka Okada,§ Shigeru Ueshima,§ Osamu Matsuo,§ Takashi Ishida,‡ Keiichi Ichimura,* and Yoichi Sakata[2†]

This study was performed to clarify the relationship between fibrinolytic components and the pathology of allergy, particularly that during the development of nasal allergy and nasal tissue changes. Intranasal OVA challenge after sensitization by i.p. administration of OVA induced a higher level of excess subepithelial collagen deposition in wild-type (WT) C57BL/6J mice than in plasminogen activator inhibitor (PAI)-1-deficient (PAI-1$^{-/-}$) mice. The excess PAI-1 induction in the nasal mucosa and higher level of active PAI-1 in the nasal lavage fluid of WT-OVA mice compared with those in WT-control mice suggested that the decrease of proteolytic activity inhibits the removal of subepithelial collagen. The frequency of sneezing, nasal rubbing, nasal hyperresponsiveness, production of specific IgG1 and IgE in the serum, and production of IL-4 and IL-5 in splenocyte culture supernatant increased significantly in WT-OVA mice. In PAI-1$^{-/-}$ mice, these reactions were absent, and specific IgG2a in serum and IFN-γ in splenocyte culture medium increased significantly. Histopathologically, there were marked goblet cell hyperplasia and eosinophil infiltration into the nasal mucosa in WT-OVA mice, but these were absent in PAI-1$^{-/-}$ mice. These results indicate that the immune response in WT-OVA mice can be classified as a dominant Th2 response, which would promote collagen deposition. In contrast, the Th2 response in PAI-1$^{-/-}$ mice was down-regulated, and the immune response shifted from Th2-dominant reaction to a Th1-dominant one. Taken together, these findings suggest that PAI-1 plays an important role not only in thrombolysis but also in immune response. *The Journal of Immunology,* **2005, 174: 8135–8143.**

Fibrinolytic components are associated with not only intravascular fibrinolysis, but also with various reactions in tissues, including ovulation, inflammation, neovascularization, tumor invasion, and tumor metastasis (1–3). Plasminogen activators (PA)[3] and their inhibitors have important roles during initiation of the fibrinolytic cascade. Two types of PA are known, the tissue-type (t-PA) and the urokinase-type (u-PA) (4), and both are glycoproteins that convert the proenzyme plasminogen into the active enzyme plasmin. The PA inhibitors (PAI) are members of the serine protease inhibitor superfamily, and they inhibit PA (5). PAI-1 appears to be the predominant physiological inhibitor of t-PA and u-PA.

In allergic diseases, tissue remodelings are observed. These changes are characterized by extracellular matrix (ECM) deposition, subepithelial fibrosis, and goblet cell hyperplasia in the airways (6, 7). It is thought that the fibrinolytic system is involved in ECM deposition and fibrosis in inflammatory tissues. Plasmin degrades fibrin and converts inactive pro-matrix metalloproteinase (MMP) into active MMP. Activated MMP degrades the ECM proteins including collagen, which is the main protein component of fibrotic tissue in the airway (8).

Fibrinolytic components have been extracted from nasal polyps (9) and the maxillary mucosa of patients with sinusitis (10), and they have been observed immunologically in human nasal mucosa (11). In addition, we demonstrated previously that expression of u-PA and PAI-1 mRNAs in human nasal tissues with allergy were enhanced, in contrast to those in normal nasal tissues (12). It was shown that the *4G* allele of the *PAI-1* gene, which is associated with elevated plasma PAI-1 level, may contribute to the development of allergic disease in humans (13, 14). Oh et al. (15) reported that up-regulation of PAI-1 synthesis occurs in lung and bronchoalveolar lavage fluids in the OVA-challenged murine asthma model and that PAI-1 promotes ECM deposition in the airways and inhibits the activity of MMPs and plasmin generation. These reports suggested that fibrinolytic components, particularly PAI-1, contribute to the development of allergic disease and changes in the allergic tissue.

To clarify the relationship between fibrinolytic components and the pathology of allergy, particularly in the development of nasal allergy and nasal tissue changes, we made a nasal allergy model with PAI-1$^{-/-}$ mice. In the present study, we used a murine model of allergic rhinitis induced by OVA.

Materials and Methods

Experimental animals and OVA sensitization

C57BL/6J PAI-1$^{-/-}$ and background-matched control mice PAI-1$^{+/+}$ (wild type; WT) were generated anew by homologous recombination in embryonic stem cells, as described previously (16, 17). Animals were maintained at the Laboratory of Experimental Medicine (Jichi Medical School, Tochigi, Japan), according to the local guidelines for animal care. Age-matched (8-wk-old, female and male) PAI-1$^{-/-}$ and WT mice were

*Department of Otorhinolaryngology-Head and Neck Surgery, and †Division of Cell and Molecular Medicine, Center for Molecular Medicine, Jichi Medical School, and ‡Department of Otorhinolaryngology, International University of Health and Welfare Hospital, Tochigi, Japan; and §Department of Physiology II, Kinki University School of Medicine, Osakasayama City, Osaka, Japan

Received for publication January 12, 2005. Accepted for publication April 8, 2005.

The costs of publication of this article were defrayed in part by the payment of page charges. This article must therefore be hereby marked *advertisement* in accordance with 18 U.S.C. Section 1734 solely to indicate this fact.

[1] This work was supported in part by Grant-in-Aid for Scientific Research No. 15591021 (to S.M.) from the Japanese Ministry of Education, Culture, Sports, Science, and Technology, and by a Health and Labor Sciences Research grant (to Y.S.) from the Japanese Ministry of Health, Labor, and Welfare.

[2] Address correspondence and reprint requests to Dr. Yoichi Sakata, Division of Cell and Molecular Medicine, Center for Molecular Medicine, Jichi Medical School, 3311-1 Yakushiji, Minamikawachi-machi, Kawachi-gun, Tochigi 329-0498, Japan. E-mail address: yoisaka@jichi.ac.jp

[3] Abbreviations used in this paper: PA, plasminogen activator; t-PA, tissue-type PA; u-PA, urokinase-type PA; PAI, PA inhibitor; ECM, extracellular matrix; MMP, matrix metalloproteinase; WT, wild type; i.n., intranasal; NLF, nasal lavage fluid; PAS, periodic acid-Schiff; SI, stimulation index.

Copyright © 2005 by The American Association of Immunologists, Inc.

0022-1767/05/$02.00

placed in one of two groups: 1) OVA group, which was given OVA sensitization by i.p. injection and then received OVA by intranasal (i.n.) challenge five times a week for 4 wk (PAI-1$^{-/-}$ and WT mice; n = 10 each); and 2) control group, which was given normal saline instead of OVA in the same schedule (PAI-1$^{-/-}$ and WT mice; n = 10 each). Under pathogen-free conditions, mice in the OVA group were sensitized using OVA as follows: 10 μg/mouse OVA (Sigma-Aldrich) diluted by sterile normal saline with 1 mg/mouse aluminum hydroxide (Sigma-Aldrich) were administered to unanesthetized mice four times by i.p. injection on days 1, 7, 14, and 21, based on the protocol of Saito et al. (18). This was followed by i.n. challenge with OVA diluted by sterile normal saline (20 μl of 25 mg/ml OVA per mouse), administered five times a week for 4 wk (Fig. 1).

Nasal symptoms and nasal responsiveness

Nasal symptoms were evaluated by counting the number of sneezes and itching motions (nasal rubbing) for 10 min after OVA i.n. provocation for the OVA group or saline i.n. provocation for the control group at the time points of days 1, 22, and 49.

Nasal responsiveness was also measured by i.n. provocation of histamine as described previously (18). After nasal challenges with 10 μl of serially diluted histamine solutions, sneezes and nasal rubbing were counted, and the time point was noted at which these were significantly higher than those associated with the normal saline control. This was expressed as the limiting concentration of histamine and measured on days 1, 22, and 49.

Tissue preparation and nasal lavage fluid (NLF) collection

At 24 h after the last i.n. provocation with OVA or saline, the mice in each group were anesthetized by i.p. injection of sodium pentobarbital (Somnopentyl; 25 mg/kg; Schering-Plough), and their four limbs were attached tightly to the cork board in a supine position with the neck hyperextended. After tracheotomy was performed in each mouse, a polyethylene catheter (inside diameter, 1.05 mm) connected to a syringe was antidromically inserted intratracheally into the choana. A 1-ml aliquot of PBS at 37°C was injected slowly into each of the nasal cavities, and the perfusate that came out of the anterior nares was collected. In this way, on average, 0.8 ml of NLF was obtained. The NLF was centrifuged (4000 × g, 10 min), and the supernatant was stored at −80°C until analysis.

After NLF collection, the spleen was aseptically removed from the animal. Subsequently, the mice were killed by exsanguination, and the nasal mucosa of five mice from each group were removed carefully. The nasal mucosa was cut to <5-mm thickness and placed in 10 vol of RNA*later* reagent (RNA stabilization reagent; Qiagen) for subsequent RNA isolation.

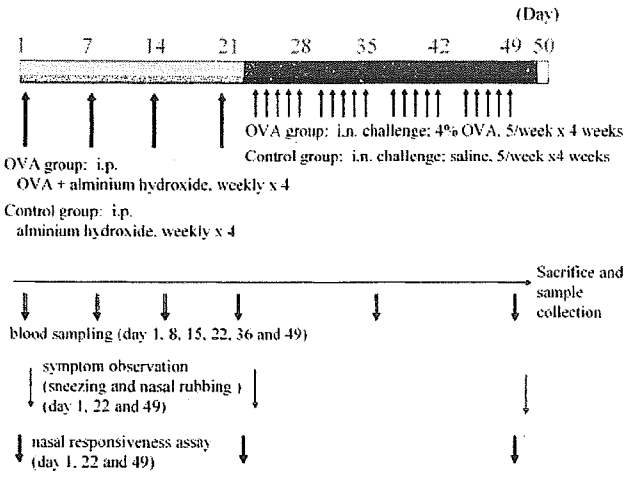

FIGURE 1. Protocol for OVA sensitization and i.n. challenge. Mice in the OVA groups were sensitized using OVA by i.p. injection on days 1, 7, 14, and 21. This was followed by administering nasal drops containing OVA, five times a week for 4 wk. Mice in the control groups were treated with diluent both during i.p. sensitization and i.n. challenge instead of OVA. Blood samples were collected on days 1, 8, 15, 22, 36, and 49. Nasal symptoms were evaluated by symptom observation (sneezing and nasal rubbing) on days 1, 22, and 49. Nasal responsiveness was also measured by i.n. provocation of histamine on days 1, 22, and 49.

For the five remaining mice of each group, perfusion fixation by 4% paraformaldehyde was performed after sacrifice. After fixation, each mouse was decapitated, and then the specimens were decalcified in 10% EDTA for 7 days.

Histopathologic analysis and immunohistochemical staining

The fixed specimens were embedded in paraffin and cut into 5-μm-thick sections. The nasal cavity was sectioned transversely at the level of the maxillary sinus. Goblet cells were quantified by the periodic acid-Schiff (PAS) reaction (19, 20). The degree of goblet cell hyperplasia was assessed by calculating the percentage of the PAS-stained area to the total resorptive epithelium area of the nasal septum. The eosinophils that infiltrated the nasal septum mucosa were counted in Luna-stained sections as described previously (21). Additionally, the neutrophils that infiltrated nasal septum mucosa were counted in May-Giemsa-stained sections.

For immunohistochemical staining, specimens embedded in paraffin were cut into 5-μm-thick sections and floated onto aminoalkylsilane-coated slides (Polysciences). The sections were deparaffinized and rehydrated. After microwave treatment, the sections were treated with 0.3% hydrogen peroxide in methanol for 15 min to inhibit the endogenous peroxidase activity of blood cells and then treated with 1% BSA in PBS (pH 7.4) containing blocking reagent for another 10 min at 25°C. An appropriate nonimmunized serum, either 1% nonimmunized rabbit serum (DakoCytomation) or 5% nonimmunized swine serum (DakoCytomation), was used as the blocking reagent. Goat polyclonal Abs against murine t-PA (Santa Cruz Biotechnology) and u-PA (Santa Cruz Biotechnology) and rabbit polyclonal Ab against murine PAI-1 (Molecular Innovations) were used for the primary Abs. For the purpose of examining subepithelial fibrosis, goat polyclonal Ab against murine collagen type I (Santa Cruz Biotechnology) and rabbit polyclonal Ab against murine collagen type III (LSL Company) were used for the primary Abs. The treated sections were incubated with the primary Abs at the appropriate concentrations (1 μg/ml anti-t-PA, 2 μg/ml anti-u-PA, 1 μg/ml anti-PAI-1, 2 μg/ml anti-collagen type I, or 1 μg/ml anti-collagen type III) in PBS with 1% BSA for 10 h at 4°C. Rabbit Ab against goat IgG labeled with HRP (DakoCytomation) and swine Ab against rabbit IgG labeled with HRP (DakoCytomation) were used for the secondary Abs. Each sample was washed extensively with PBS containing Triton X-100 and then incubated with the secondary Abs at the appropriate concentrations (2 μg/ml anti-goat IgG or 1 μg/ml anti-rabbit IgG Abs) in PBS with 1% BSA for 1 h at 24°C. After washing again, immunoreactive sites were visualized with hydrogen peroxide and diaminobenzidine and then counterstained with hematoxylin. Control sections were incubated with 5 μg/ml nonimmune rabbit IgG (DakoCytomation) or 5 μg/ml nonimmune goat IgG (DakoCytomation) instead of the primary Abs, respectively.

Real-time RT-PCR

To evaluate the production of fibrinolytic components (t-PA, u-PA, and PAI-1) in nasal mucosa, we examined the presence of mRNA of mouse t-PA, u-PA, and PAI-1 by real-time RT-PCR. The nasal tissues for RNA isolation (20–30 μg) were homogenized, and total RNA was isolated by using the RNeasy Mini kit (Qiagen) as described previously (12, 22, 23). Total RNA (0.5 μg) from each sample was reverse transcribed as described previously (12). Real-time quantitative PCR was performed using a TaqMan Gold RT-PCR kit (PerkinElmer Applied Biosystems) and an ABI Prism 7700 Sequence Detection System (PerkinElmer Applied Biosystems) (12, 24). Amplified PCR products were resolved in 2% agarose gels.

Table I. *RT-PCR primer and probe sequences for mouse fibrinolytic components and GAPDH*

Primer	Sequence
t-PA	Sense: 5′-GGCACGACACAATTATTGTCGG-3′
	Antisense: 5′-GCTTTCGGTCCTTCATCACATG-3′
	Probe: 5′-ATCCAGATGGTGATGCCAGACCTTGGTG-3′
u-PA	Sense: 5′-ACCAACAAGGCTTCCAGTGTG-3′
	Antisense: 5′-TCAGTGAATTCTCCCCCAACA-3′
	Probe: 5′-CAGAAGGCTCTAAGGCCCCGCTTTAAGA-3′
PAI-1	Sense: 5′-ACTGTCCTATCTCAAGGTCCACTGT-3′
	Antisense: 5′-TGATCTGTCTATCCGTTGCCC-3′
	Probe: 5′-AAATGTCCACCTTGCCCACCTCCA-3′
GAPDH	Sense: 5′-ATGGCCTTCCGTGTTCCTA-3′
	Antisense: 5′-ATACTTGGCAGGTTTCTCCAGG-3′
	Probe: 5′-CCAATGTGTCCGTCGTGGATCTGA-3′

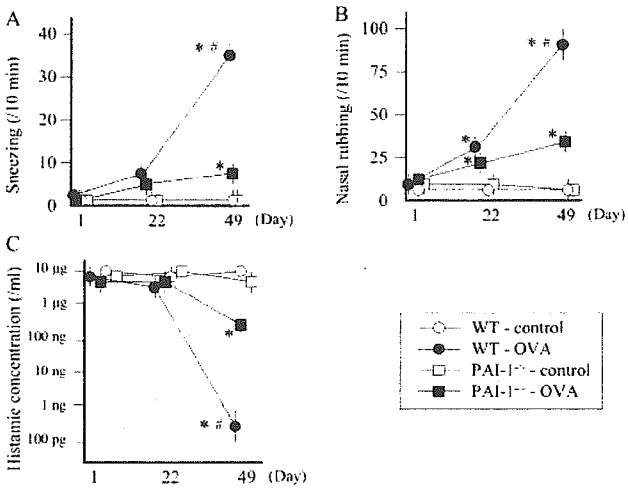

FIGURE 2. Nasal symptoms and nasal histamine responsiveness in WT and PAI-$1^{-/-}$ mice. Nasal symptoms were evaluated by counting the number of sneezes (*A*) and itching motions (*B*) for 10 min after OVA i.n. provocation for each group on days 1, 22, and 49. Nasal histamine responsiveness (*C*) was expressed as the minimum concentration of histamine that caused both sneezing and nasal rubbing on days 1, 22, and 49. Values are means ± SEM of 10 samples in each group. *, $p < 0.01$ when compared with each control group at the same day point. #, $p < 0.01$ when compared with PAI-$1^{-/-}$-OVA group at the same day point.

stained with ethidium bromide, and photographed under UV light. The reverse transcriptase enzyme was omitted from the cDNA synthesis for each specimen to serve as a negative control.

The respective primers and probes for t-PA (25), u-PA (26), PAI-1 (27), and GAPDH (28) used in this study were chosen with the assistance of the computer program Primer Express (PerkinElmer Applied Biosystems). We conducted BLASTN searches to confirm the total gene specificity of the nucleotide sequences chosen for the primers and probes and the absence of DNA polymorphisms. Primers were purchased from Invitrogen Life Technologies, and the probes were purchased from PerkinElmer Applied Biosystems. These sequences are listed in Table I.

PAI-1 ELISA and PAI-1 activity assay in NLF

According to the manufacturer's instructions, NLF were assayed for PAI-1 total protein by a sandwich ELISA kit (Molecular Innovations) and analyzed for active PAI-1 by a PAI-1 activity assay kit (Molecular Innovations). The lower limit of detection for both assays was 0.05 ng/ml.

Measurement of OVA-specific IgG1, IgG2a, and IgE levels, and total IgE

OVA-specific IgG1, IgG2a, and IgE levels were measured by ELISA. Blood samples were collected from the tail at the time points of days 1, 8, 15, 22, 36, and 49. The 96-well polystyrene microtiter plates (Nunc) were coated with OVA (5 µg/ml) in PBS (pH 7.2) for 24 h at 4°C. Nonspecific sites were blocked with PBS containing 20% skim milk (Difco Laboratories). Serum samples diluted in the blocking buffer (1/800 for IgG1, 1/300 for IgG2a, and 1/10 for IgE Abs) were incubated for 2 h at 24°C. Subsequently, for IgG1 and IgG2a, stock solutions of rabbit anti-mouse IgG1 and IgG2a Abs (Bio-Rad Laboratories) were added, respectively, and incubated for 2 h at 24°C. Bound Ig were detected using either peroxidase-conjugated goat anti-rabbit IgG Ab (2 µg/ml) (BioSource International) or goat anti-mouse IgE Ab (1 µg/ml) (Bethyl Laboratories) and ABTS/H_2O_2 (Kirkegaard & Perry Laboratories) as substrate. OD_{405} were measured.

Total IgE Abs were measured by a sandwich ELISA using the mouse IgE ELISA quantitation kit (Bethyl Laboratories) according to the manufacturer's instructions. The enzymatic activity was measured using ABTS/H_2O_2 (Kirkegaard & Perry Laboratories) as substrate. OD_{405} was measured, and IgE concentrations were determined by interpolation from a standard curve performed with purified mouse IgE.

Proliferation assays

Preparation of splenocytes and proliferation assay were performed as described previously (29). In brief, the spleen was removed from the animal and then minced and forced through a mesh. After erythrocytes were lysed, the cells were washed and resuspended in the medium, RPMI 1640 (Invitrogen Life Technologies), containing 10% FBS, 20 µg/ml penicillin, and 20 µg/ml streptomycin. Spleen cells (10^6/ml, 0.1 ml/well) were plated into 96-well plates and stimulated with PHA (50 µg/ml) and OVA (500, 50, 5, and 0.5 µg/ml) for 72 h. As the control, cells were incubated with only the medium. Thereafter, cultures were pulsed with 1 µCi/well [^{3}H]thymidine (Amersham Biosciences) for 16 h. Cells were harvested, and their [^{3}H]thymidine uptake was measured by scintillation counting. Proliferative responses were calculated as the means of triplicate wells and were expressed as the stimulation index (SI). A SI of >2 was considered positive.

Cytokine assays

Spleen cells (10^6/ml, 1 ml/well) were plated in 24-well plates and stimulated with 50 µg/ml OVA. After 48 h, supernatants were taken and stored at −80°C until analysis. The levels of IL-4, IL-5, and IFN-γ in the supernatants and NLF were measured by sandwich ELISA using the mouse IL-4, IL-5, and IFN-γ ELISA Biotrack system kit (Amersham Biosciences) according to the manufacturer's instructions.

Statistical analysis

Results were compared using one-way ANOVA for nasal symptoms, nasal histamine responsiveness, Ab levels, and proliferation assays. Except for these experiments, unpaired Student's *t* test was used to compare data between observations in PAI-$1^{-/-}$ and WT mice. Differences were considered significant for p values <0.01.

Results

Clinical symptoms and nasal responsiveness

Nasal symptoms, sneezing and nasal rubbing, were observed for 10 min after i.n. challenge at the time points of days 1, 22, and 49.

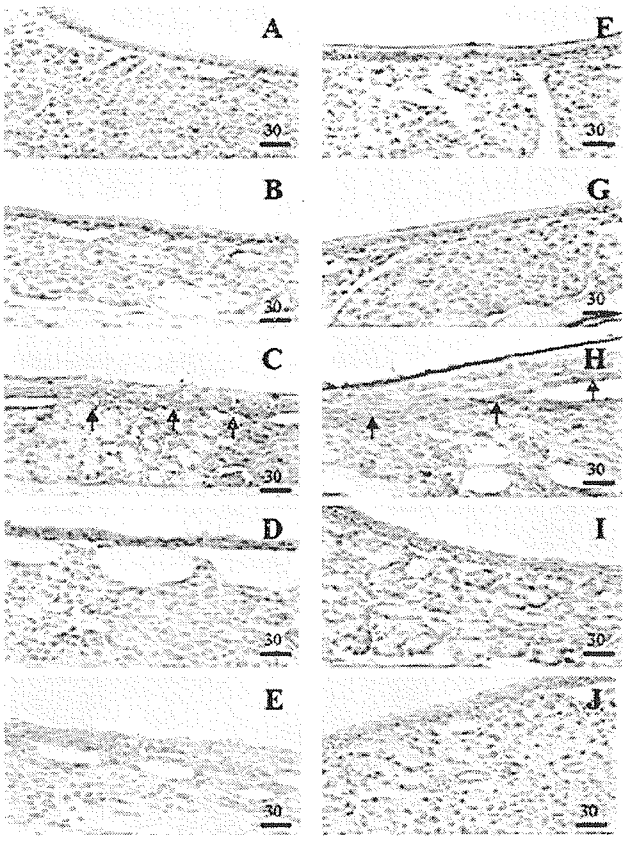

FIGURE 3. Immunohistochemical staining of collagen types I and III in mouse nasal mucosa. Control sections treated with nonimmune goat IgG (*A*) or nonimmune rabbit IgG (*F*) were devoid of stain. Sections were immunostained with anti-collagen type I (*B–E*) and anti-collagen type III (*G–J*), respectively. Figures show the nasal mucosa of WT control (*B* and *G*), WT OVA (*C* and *H*), PAI-$1^{-/-}$ control (*D* and *I*), and PAI-$1^{-/-}$ OVA (*E* and *J*). Arrows indicate positive staining. Bars, 30 µm.

As shown in Fig. 2, *A* and *B*, nasal symptoms were accelerated significantly in the WT-OVA group. The frequency of sneezes and nasal rubs were 4-fold less in the PAI-1$^{-/-}$-OVA group than in the WT-OVA group on day 49. The dose of histamine inducing nasal hyperresponsiveness in the PAI-1$^{-/-}$-OVA group was at least 1000-fold lower than that in the WT-OVA group after OVA challenge (Fig. 2*C*).

Immunohistochemical staining of collagen

Immunohistochemistry for collagen types I and III in the WT-OVA group showed strong immunoreactivity in the subepithelial region (Fig. 3, *C* and *H*). Additionally, numerous collagen bundles were observed clearly throughout the interstitial submucosal tissue. In the sections from the other groups of mice, the submucosal tissue only showed weak immunoreactivities for collagen types I and III (Fig. 3, *B*, *D*, *E*, *G*, *I*, and *J*).

The expression of fibrinolytic components mRNA in nasal mucosa

As shown in Fig. 4*A*, t-PA mRNA expression significantly decreased in the WT-OVA group compared with that in the WT-control group. However, there was no significant difference in t-PA mRNA expression between the PAI-1$^{-/-}$-OVA group and PAI-1$^{-/-}$-control group. Interestingly, the level of u-PA mRNA was higher in the WT-OVA group than the WT-control group. Even more notably, in the PAI-1$^{-/-}$ mice, the u-PA level of the OVA sensitization group did not increase, being significantly lower than that in the WT-OVA group (Fig. 4*B*). PAI-1 mRNA expression significantly increased in the WT-OVA group compared with that in the WT-control group (Fig. 4*C*).

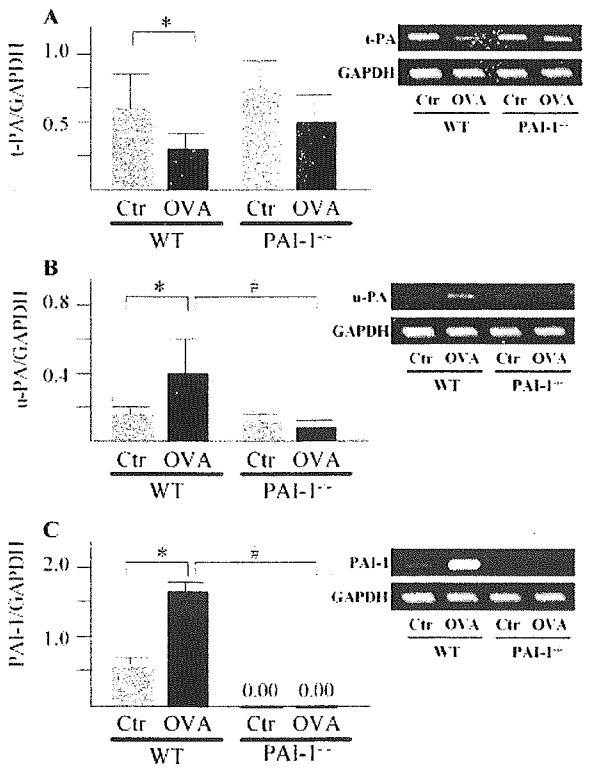

FIGURE 4. Fibrinolytic components mRNA expression in mouse nasal mucosa. Quantitative real-time RT-PCR was performed for t-PA (*A*), u-PA (*B*), and PAI-1 (*C*) mRNA in each group. In addition, representative electrophoretic patterns of PCR products are shown. Values are means ± SEM of five samples for each group. Ctr, Control. *, $p < 0.01$ when compared with each control group. #, $p < 0.01$ when compared with the PAI-1$^{-/-}$-OVA group.

Immunohistochemical staining of fibrinolytic components

In murine nasal mucosa, t-PA-immunoreactive material was localized predominantly in the epithelium (Fig. 5, *B–E*). t-PA staining in the epithelium of the WT-OVA mice was weaker than that of the WT-control mice (Fig. 5, *B* and *C*). In contrast, the PAI-1 signal in the submucosal gland of the WT-OVA group was much stronger than that in the WT-control mice (Fig. 5, *L* and *M*). In addition, positive staining of u-PA was noted exclusively in the epithelium and the submucosal glands in the WT-OVA group (Fig. 5, *G–J*). These histological data on the fibrinolytic components in the WT-OVA group was almost the same as what was observed in the nasal mucosa of human allergic patients (12). Surprisingly, the u-PA signal was very weak in PAI-1$^{-/-}$ mice (Fig. 5, *I* and *J*).

PAI-1 level and activity in NLF

To examine PAI-1 production and activity in OVA-challenged murine nose, PAI-1 ELISA and PAI-1 activity assay were performed. The level of PAI-1 total protein in the NLF from the WT-OVA group was 5-fold higher than that from the WT-control group (Fig. 6*A*). The active PAI-1 in the NLF from the WT-OVA group was 5-fold greater than that from the WT-control group (Fig. 6*B*). No active PAI-1 and PAI-1 total protein were detected in the NLF from PAI-1$^{-/-}$ mice after challenge with OVA or saline.

Serum OVA-specific IgG1, IgG2a, and IgE levels, and total IgE

The WT-OVA group developed high levels of specific IgG1 and IgE Abs in sera (Fig. 7, *A* and *C*), and little or no OVA-specific IgG2a production was observed (*B*). In the PAI-1$^{-/-}$-OVA group, the levels of specific IgG1 and IgE Abs in sera, although higher than those of the control group, were far less than those in the WT-OVA group. In contrast, only the PAI-1$^{-/-}$-OVA group had a high serum level of specific IgG2a Ab. The increase of OVA-specific IgE levels was parallel to that in total IgE concentration in mouse sera (Fig. 7*D*).

Cytokine profile

To determine whether cytokines were present in the nasal cavity during development of allergy to OVA, we collected NLF from mice in each group and measured the levels of IL-4, IL-5, and IFN-γ. The levels of IL-4 and IL-5 in the NLF from the WT-OVA group were significantly higher than those from the PAI-1$^{-/-}$-OVA group. Conversely, the NLF from the PAI-1$^{-/-}$-OVA group contained a higher level of IFN-γ than those from the WT-OVA group (Table II). To determine the systemic lymphocyte cytokine secretion profiles, supernatants from cultured lymphocytes stimulated with OVA were harvested and assayed for IL-4, IL-5, and IFN-γ. The lymphocytes from the WT-OVA group produced significantly higher levels of IL-4 and IL-5 compared with those from the PAI-1$^{-/-}$-OVA group. Conversely, OVA-stimulated cells from the PAI-1$^{-/-}$-OVA group had a significantly higher level of IFN-γ than those from the WT-OVA group (Table II).

Proliferation response

To evaluate the role of T cells in the development of allergy to OVA, we determined the lymphoproliferative response from splenocytes after in vitro stimulations. Spleen cells from mice in the WT-OVA group showed a significant dose-dependent proliferative response to OVA stimulation (Fig. 8). In particular, when the OVA concentration was >5 μg/ml, the SI in the WT-OVA group was >2 and significantly increased in comparison with that

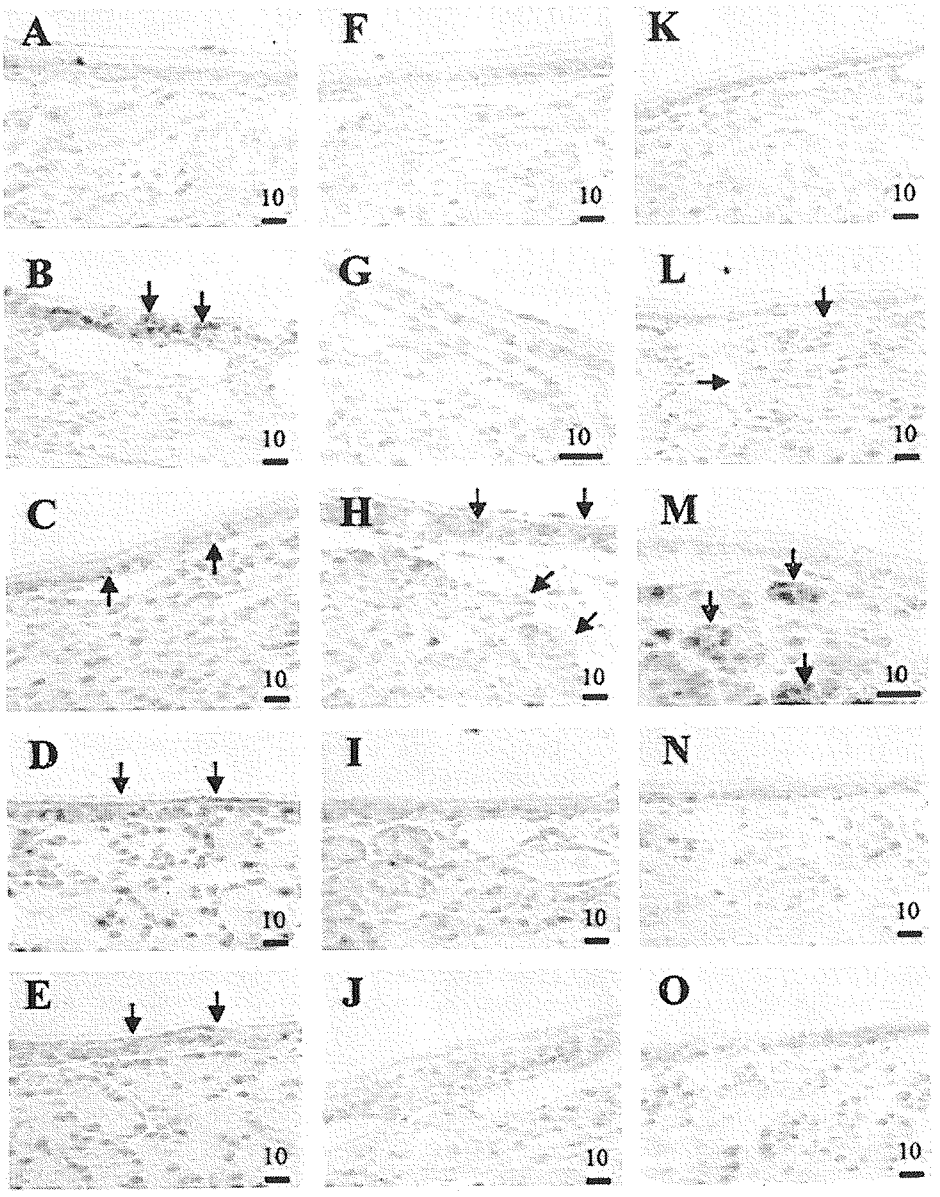

FIGURE 5. Immunohistochemical staining of fibrinolytic components in mouse nasal mucosa. Control sections treated with nonimmune goat IgG (*A* and *F*) or nonimmune rabbit IgG (*K*) were devoid of stain. Sections were immunostained with anti-t-PA (*B–E*), anti-u-PA (*G–J*), and anti-PAI-1 (*L–O*), respectively. Figures show the nasal mucosa of WT-control (*B*, *G*, and *L*), WT-OVA (*C*, *H*, and *M*), PAI-1$^{-/-}$-control (*D*, *I*, and *N*), and PAI-1$^{-/-}$-OVA (*E*, *J*, and *O*). Arrows indicate positive staining. Bars, 10 μm.

in the WT-control group ($p < 0.05$). In other groups, including PAI-1$^{-/-}$ mice, the SI did not exceed 2 at any concentration.

Pathological changes in nasal mucosa

We examined goblet cell hyperplasia and eosinophilic infiltration in nasal mucosa to judge whether allergic inflammation occurred in the nasal cavity of mice (Fig. 9). The examination of PAS-stained sections revealed that the Ag challenge in the WT-OVA group induced a marked goblet cell hyperplasia in the resorptive epithelium of the nasal cavity (Fig. 9, *A* and *B*). Hyperplasia in the WT-OVA group was more outstanding than that in the PAI-1$^{-/-}$-OVA group (Fig. 9, *C* and *D*). The number of eosinophils infiltrating the nasal septum mucosa was 30-fold less in the PAI-1$^{-/-}$-OVA group than in the WT-OVA group (Fig. 9, *E–H*). In contrast, only a few neutrophils infiltrated the nasal septum mucosa, and there was no significant difference between each group in the number. The quantification data of goblet cell hyperplasia and cellular infiltration are shown in Table III.

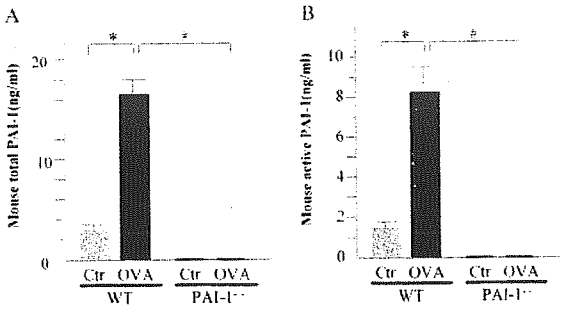

FIGURE 6. PAI-1 level and activity in NLF. NLF were assayed for PAI-1 total protein by sandwich ELISA (*A*), and for active PAI-1 by PAI-1 activity assay (*B*). Values are means ± SEM of five samples for each group. Ctr, Control. *, $p < 0.01$ when compared with each control group. #, $p < 0.01$ when compared with the PAI-1$^{-/-}$-OVA group.

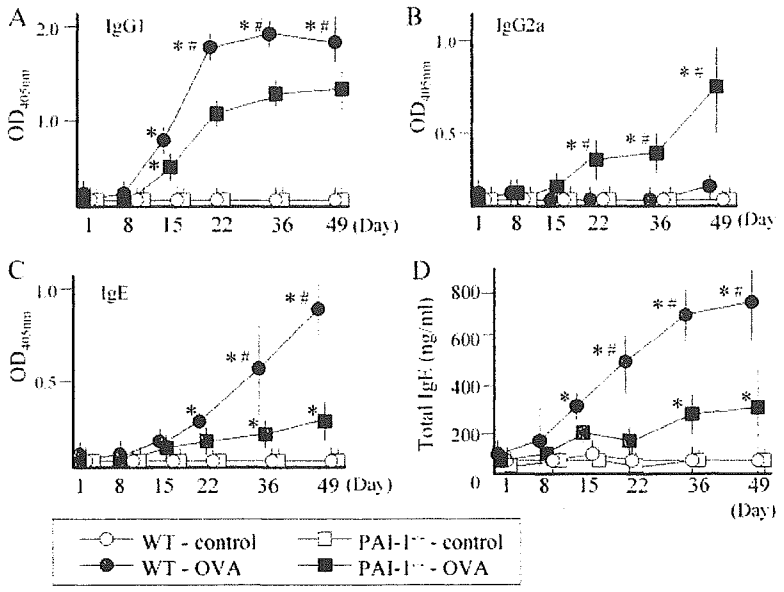

FIGURE 7. Time course and levels of OVA-specific IgG1, IgG2a, and IgE, and total IgE in sera of mice. *A*, Specific IgG1; *B*, specific IgG2a; *C*, specific IgE; and *D*, total IgE. Values are means ± SEM of 10 samples in each group. *, $p < 0.01$ when compared with each control group at the same day point. #, $p < 0.01$ when compared with the PAI-$1^{-/-}$-OVA group (*A*, *C*, and *D*) or when compared with the WT-OVA group (*B*) at the same day point.

Discussion

The PA-plasmin system plays an important role in inflammation as well as intravascular fibrinolysis. Inflammation in diseases such as allergy consists of various phases, cellular infiltration, fibrosis, edema, and tissue remodeling. Although the effects of fibrinolytic components in allergy are still obscure, we can assume that these components may be significant factors in each phase of allergy, because previous studies have shown the involvement of the PA-plasmin system in each phenomenon of inflammation (2, 12, 30).

In this study, we demonstrated that WT mice can develop nasal allergy for OVA, but the PAI-1^{-} mice cannot. The clinical symptoms of allergy in our system were defined to be sneezing and nasal rubbing. As shown in Fig. 2, local administration of OVA induced allergic symptoms in sensitized mice.

Previous studies have shown subepithelial depositions of collagen types I and III in bronchial biopsy specimens of asthma patients and allergic nasal mucosa that correlate with airway hyperresponsiveness (31, 32). As shown in Fig. 3, excess amounts of brown-stained type I and type III collagen are found in the nasal mucosa obtained from OVA-challenged WT mice in our system. In contrast, the collagen deposition in the nasal mucosa from OVA-challenged PAI-$1^{-/-}$ mice appeared less significant than that in the OVA-challenged WT mice. Interestingly, in this mouse model, at the local sensitization termination point (day 49), nasal sensitivity not only to histamine but also to OVA correlates with the accumulation of collagen (Fig. 2). Using WT and PAI-$1^{-/-}$ mice, Hattori et al. (33) in the bleomycin-induced pulmonary fibrosis model and Oh et al. (15) in the OVA-induced asthma model observed the similar effect of PAI-1 on excess fibrous material accumulation in mouse lung tissues. PAI-1 is the primary physiological inhibitor of both u-PA and t-PA. PA converts the inactive proenzyme plasminogen to plasmin, a protease of fairly broad substrate specificity, and then plasmin and metalloprotease activated by plasmin are supposed to play a central role in the concerted immune response of the cell to degrade matrix proteins and cross tissue planes (15). We thus examined the effect of PAI-1 deficiency on the production of PA in mouse nasal mucosa. As shown in Fig. 4, u-PA and PAI-1 mRNA levels of the WT-OVA group were significantly higher than those of the control mice group. However, the t-PA mRNA was significantly down-regulated. In contrast, the t-PA mRNA level in PAI-$1^{-/-}$ mice was not significantly different between the OVA-sensitized group and the non-sensitized control group. The u-PA mRNA level of PAI-$1^{-/-}$-OVA mice was significantly lower than that of WT-OVA mice.

Table II. *Cytokine assays of NLF and lymphocyte culture supernatant*

Group	IL-4	IL-5	IFN-γ (pg/ml)
NLF			
WT-control	0.6 ± 0.9[a]	1.8 ± 1.9	0.8 ± 0.8
WT-OVA	46.2 ± 13.7 *	38.8 ± 16.6 *	10.4 ± 16.8 *
PAI-$1^{-/-}$-control	1.2 ± 1.1	0.6 ± 0.9	1.0 ± 0.7
PAI-$1^{-/-}$-OVA	10.8 ± 9.1 * *	4.6 ± 4.1 * *	372 ± 169 * *
Lymphocyte culture supernatant			
WT-control	1.4 ± 0.9	0.8 ± 0.8	0.8 ± 0.8
WT-OVA	525 ± 170 *	114 ± 13.4 *	9.4 ± 17.2 *
PAI-$1^{-/-}$-control	0.8 ± 0.8	1.0 ± 2.2	1.2 ± 0.8
PAI-$1^{-/-}$-OVA	25.6 ± 15.7 * *	14.2 ± 7.2 * *	1044 ± 608 * *

[a] Values are means ± SEM of five samples in each group.
*, $p < 0.01$.

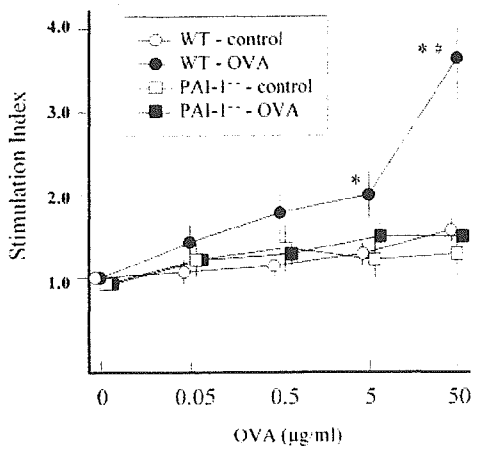

FIGURE 8. Proliferation of splenocytes following stimulation with OVA. Splenocytes were cultured in triplicate at 1×10^6 cells/ml. Results are expressed as the SI. Values are means ± SEM of 10 samples in each group. *, $p < 0.01$ when compared with the WT-control group at the same OVA concentration. #, $p < 0.01$ when compared with the PAI-$1^{-/-}$-OVA group at the same OVA concentration.

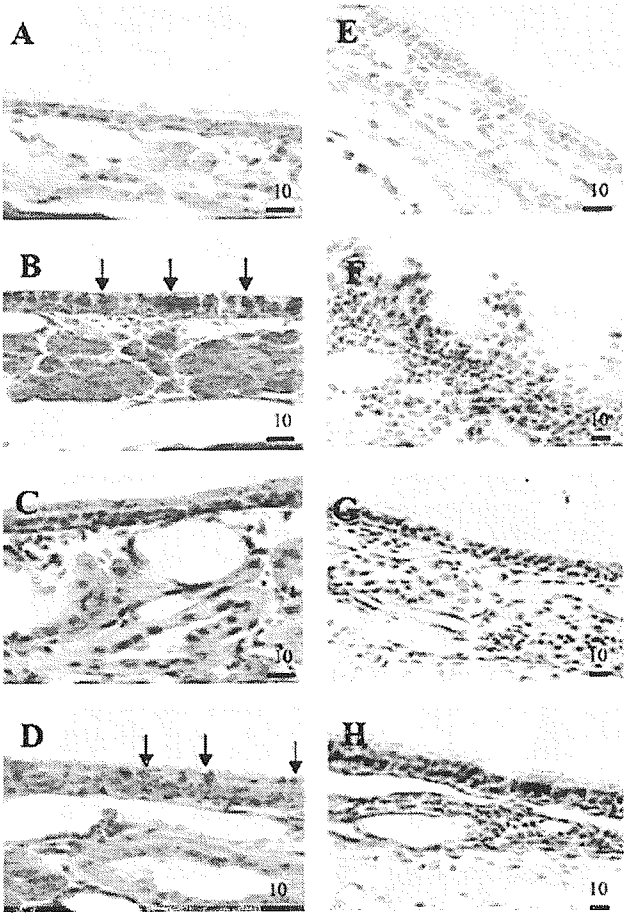

FIGURE 9. Pathological changes in mouse nasal mucosa. The sections were stained with the PAS histochemical reaction in the WT-control (*A*), WT-OVA (*B*), PAI-$1^{-/-}$-control (*C*), and PAI-$1^{-/-}$-OVA (*D*) groups, respectively. Luna staining was performed in nasal mucosa for the WT-control (*E*), WT-OVA (*F*), PAI-$1^{-/-}$-control (*G*), and PAI-$1^{-/-}$-OVA (*H*) groups, respectively. *A–D*. Arrowheads indicate mucus in goblet cells of the epithelium and mucinous cells of the submucosal gland (PAS positive). Bars, 10 μm.

The PAI-$1^{-/-}$ mice definitely had a lower level of u-PA mRNA, because this was also confirmed by the immunostaining study on the nasal mucosa (Fig. 5). However, the net PA activity in PAI-$1^{-/-}$ mice should not be lower than that in WT mice, because there was almost no inhibitor of u-PA in PAI-$1^{-/-}$ mice, and PAI-1 mRNA and protein were significantly increased in WT-OVA mice. In addition, in WT-OVA mice, active PAI-1 levels, meaning the residual antiproteolytic activity of PAI-1 after interaction with PA, were also higher than those in the saline-challenged mice (Fig. 6*B*). In the nasal septum, there was a small number of mast cells, which were suggested as PAI-1 source in asthma (34), and neutrophils; we could not find any significant difference in the number of these cells among the WT-OVA mice and other genotypes of mice (Table III). Although many cytokines, released from white blood cells, would be involved in the up-regulation of the PAI-1 production, the main source of PAI-1 may be the nasal submucosal gland, as shown in Fig. 5*M*. Taken together, these observations would suggest that inhibition of proteolytic activity by abnormal induction of PAI-1 decreases the MMP activation and collagen removal in allergic rhinitis. In this scenario, however, PAI-1 plays rather a secondary role. Is there another possible mechanism in which PAI-1 may have a major role in promoting collagen deposition? In type I allergy, including allergic rhinitis, increased serum IgE is characteristic of the immune reaction after exposure to an Ag. In mice, the Th2 response results in IgG1 and IgE production, whereas the Th1 response leads to IgG2a synthesis (35). Allergic rhinitis is hence considered to be a result of Th2 cell activation. The significantly increased productions of IgE and IgG1 and the low levels of IgG2a in WT-OVA mice immunized and challenged with OVA (Fig. 7, *A–C*) implicated the Th2 response against this allergen. In contrast, high levels of specific IgG1 and IgE were nearly absent in PAI-$1^{-/-}$-OVA mice. Conversely, only the PAI-$1^{-/-}$-OVA group showed a significant increase in the level of specific IgG2a. Thus, these results indicate that down-regulation of the Th2 immune response in PAI-$1^{-/-}$ mice brings about an inappropriate overactivation of the Th1 immune response to the Ag, which would otherwise induce the Th2 response instead. Considering the importance of the Th2 phenotype for development of fibrotic pulmonary and extrapulmonary complications (36), it is possible that the Th2 phenotype itself would promote collagen deposition in the WT compared with PAI-$1^{-/-}$ mice. The change of immune responsiveness in PAI-$1^{-/-}$ mice was also confirmed in the cytokine profiles of the NLF (local) and the supernatant of the cultured lymphocytes of the spleen (systemic) from mice challenged by OVA. The levels of IL-4 and IL-5 in the supernatant of OVA-stimulated lymphocyte cultures from WT-OVA mice were 10–20 times higher than those from PAI-$1^{-/-}$-OVA mice. OVA-stimulated cells from PAI-$1^{-/-}$-OVA mice had a 100-fold higher level of IFN-γ than those from WT-OVA mice. The tendencies of these cytokine profiles were also reflected in the splenocyte proliferation assay from the conditioned mice (Fig. 8). These results show that the sensitized group exhibited each immune reaction not only locally but also systemically, explaining the high level of IgE in the WT-OVA mice. The high level of IL-4 would induce high-level Ab production, including IgE as described previously (37, 38), in the nasal cavity, thereby contributing to the immediate-type allergic reaction after Ag inhalation. In contrast, IL-5 has highly specific effects on eosinophilic proliferation, migration, activation, and survival (39, 40). The high level of IL-5 would be responsible for the infiltration of eosinophils into the nasal mucosa (Fig. 9*F*). As for the hyperplasia of goblet cells in sensitized mice (Fig. 9*B*), a similar tissue change is observed in human allergic rhinitis (12).

Table III. *Goblet cell hyperplasia and cellular infiltration in nasal mucosa*

Group	Goblet Cells[a] (% of PAS area)	Eosinophilic Infiltration[b] (cells/mm^2)	Neutrophilic Infiltration[c] (cells/mm^2)
WT-control	8.1 ± 1.1[d] *	0.2 ± 0.4 *	3.0 ± 0.8
WT-OVA	58.3 ± 17.2 *	390 ± 70.3 *	5.7 ± 2.5
PAI-1$^{-/-}$-control	9.9 ± 4.7 *	0.8 ± 1.7 *	3.3 ± 0.9
PAI-1$^{-/-}$-OVA	27.8 ± 6.7 *	13.6 ± 4.9 *	5.0 ± 3.1

[a] Degree of goblet cells hyperplasia was shown by calculating percentage of PAS area to total resorptive epithelium area of nasal septum.
[b] The eosinophils that infiltrated nasal septum mucosa were counted in Luna-stained sections.
[c] The neutrophils that infiltrated nasal septum mucosa were counted in May-Giemsa-stained sections.
[d] Values are means ± SEM of five samples in each group.
*, $p < 0.01$.

Surprisingly, in PAI-1$^{-/-}$-OVA mice, however, there was almost none of these mucosal changes (Fig. 9, *D* and *H*).

These histological data and cytokine profiles indicated that mice deficient in PAI-1 fail to generate the Th2 immune response to OVA challenge. Gyetko et al. (41, 42) have reported that u-PA is required to generate both the Th1 and Th2 immune responses to infection. Does this mean that down-regulation of the Th2 immune response in PAI-1$^{-/-}$ mice was induced through a low level of u-PA? This seems unlikely, because although the PAI-1$^{-/-}$ mice had a lower level of u-PA message than WT mice, the u-PA activity in PAI-1$^{-/-}$ mice should be higher than that in WT mice as described above. PAI-1 works not only as a serine protease inhibitor to prevent the ECM degradation, but acts as a de-adhesion molecule to detach cells attached to vitronectin via integrins (43). In addition, the de-adhesive activity of PAI-1 does not require its interaction with vitronectin. However, there is an absolute requirement for its binding to uPA. Free u-PA or PAI-1 with vitronectin has only weak detachment activity (44). The loss of detachment activity in PAI-1$^{-/-}$ mice might explain the inhibition of cell movement, including eosinophil infiltration. This detachment profile may change the signal transduction of leukocytes through cell-to-cell and cell-to-ligand interactions. Many reports suggest that malignant cells expressing more PAI-1 can metastasize more efficiently than tumors with less PAI-1 production (1). In addition, there are clinical reports that higher level of active PAI-1 in plasma due to the 4G/5G polymorphism of the *PAI-1* gene is related closely to allergic disease (45–47). These reports, in conjunction with our study, support that PAI-1 is a rather critical regulator of some immune response for Ag stimulation. Observing the similar PAI-1-dependent deposition of collagen in the lung, Oh et al. (15) reported no significant difference in the numbers of peribronchial eosinophils and goblet cells and OVA-specific IgE levels after OVA challenge. There are differences in the target organ (the lung in the study by Oh et al. (15) and the nose in our study), in frequency of immunization with OVA (two to four times for 3 wk), in challenge frequency (three to five times a week for 4 wk), and in the area of lavage fluid collection (lung and nose). We do not know the exact reason for the discrepancy between their observation and ours. However, there may be differences in receptor and ligand distribution between the upper and lower airways and in the specificity of lavage fluid collection (48), because the numbers of eosinophils and goblet cells as well as OVA-specific IgE were more greatly increased in the OVA-challenged PAI-1$^{-/-}$ mice than in the saline-challenged control, although the levels were significantly lower than those in OVA-challenged WT mice in our system.

In summary, we show that allergic rhinitis is restrained in OVA sensitization of PAI-1-deficient mice, and the immune response characteristics tend to shift from a Th2-dominant reaction to a Th1-dominant reaction. These findings, with other previous works, demonstrate that fibrinolytic components including PAI-1 play an important role not only in thrombolysis and proteolysis, but also in the immune response by changing the balance between the Th2 reaction and the Th1 reaction.

Acknowledgments

We are grateful to Dr. Stephanie M. Jung for critical reading of the manuscript.

Disclosures

The authors have no financial conflict of interest.

References

1. Dano, K., P. A. Andreasen, J. Grondahl-Hansen, P. Kristensen, L. S. Nielsen, and L. Skriver. 1985. Plasminogen activators, tissue degradation and cancer. *Adv. Cancer Res.* 44: 139–266.
2. Loskutoff, D. J., M. Sawdey, and J. Mimuro. 1989. Type 1 plasminogen activator inhibitor. *Prog. Hemost. Thromb.* 9: 87–115.
3. Carmeliet, P., and D. Collen. 1995. Gene targeting and gene transfer studies of the plasminogen/plasmin system: implications in thrombosis, hemostasis, neointima formation, and atherosclerosis. *FASEB J.* 9: 934–938.
4. Saksela, O., and D. B. Rifkin. 1998. Cell-associated plasminogen activation: regulation and physiological functions. *Annu. Rev. Cell Biol.* 4: 93–126.
5. Kawano, T., K. Morimoto, and Y. Uemura. 1968. Urokinase inhibitor in human placenta. *Nature* 217: 253–254.
6. Holgate, S. T. 1998. Airway remodeling. *Eur. Respir. Rev.* 8: 1007–1011.
7. Bousquet, J., P. K. Jeffery, W. B. Busse, M. Johnson, and A. M. Vignola. 2000. Asthma: from bronchoconstriction to airway remodeling. *Am. J. Respir. Crit. Care Med.* 61: 1720–1745.
8. Collen, D. 1999. The plasminogen (fibrinolytic) system. *Thromb. Haemost.* 82: 259–270.
9. Yamashiro, Y., M. Nakamura, G. W. Huang, and T. Kosugi. 1992. Presence of urokinase type plasminogen activator (u-PA) in tissue extracts of antrochoanal polyp. *Laryngoscope* 102: 1049–1052.
10. Hamaguchi, Y., M. Ohi, Y. Sakakura, and Y. Miyoshi. 1985. Purification and characterization of tissue-type plasminogen activator in maxillary mucosa with chronic inflammation. *Thromb. Haemost.* 54: 485–489.
11. Yasuda, T., Y. Sakata, S. Madoiwa, J. Mimuro, M. Matsuda, and K. Kitamura. 1998. Fibrinolytic components in nasal mucosa and nasal secretion. *Histochem. Cell Biol.* 110: 449–455.
12. Sejima, T., S. Madoiwa, J. Mimuro, T. Sugo, T. Ishida, K. Ichimura, and Y. Sakata. 2004. Expression profiles of fibrinolytic components in nasal mucosa. *Histochem. Cell Biol.* 122: 61–73.
13. Cho, S. H., I. P. Hall, M. Wheatley, J. Dewar, D. Abraha, J. D. Mundo, H. Lee, and C. K. Oh. 2001. Possible role of the 4G/5G polymorphism of the plasminogen activator inhibitor 1 gene in the development of asthma. *J. Allergy Clin. Immunol.* 108: 212–214.
14. Bucková, D., L. Izakovicova Hollá, and J. Vácha. 2002. Polymorphism 4G/5G in the plasminogen activator inhibitor-1 (PAI-1) gene is associated with IgE-mediated allergic diseases and asthma in the Czech population. *Allergy* 57: 446–448.
15. Oh, C. K., B. Ariue, R. F. Alban, B. Shaw, and S. H. Cho. 2002. PAI-1 promotes extracellular matrix deposition in the airways of a murine asthma model. *Biochem. Biophys. Res. Commun.* 294: 1155–1160.
16. Carmeliet, P., L. Kieckens, L. Schoonjans, B. Ream, A. V. Nuffelen, G. Prendergast, M. Cole, R. Bronson, D. Collen, and R. C. Mulligan. 1993. Plasminogen activator inhibitor-1 gene-deficient mice. I. Generation by homologous recombination and characterization. *J. Clin. Invest.* 92: 2746–2755.

17. Carmeliet, P., J. M. Stassen, L. Schoonjans, B. Ream, J. J. van den Oord, M. De Mol, R. C. Mulligan, and D. Collen. 1993. Plasminogen activator inhibitor-1 gene-deficient mice. II. Effect on hemostasis, thrombosis, and thrombolysis. *J. Clin. Invest.* 92: 2756–2760.
18. Saito, H., K. Howie, J. Wattie, A. Denburg, R. Ellis, M. D. Inman, and J. A. Denburg. 2001. Allergen-induced murine upper airway inflammation: local and systemic changes in murine experimental allergic rhinitis. *Immunology* 104: 226–234.
19. Nettleton, G. S., and A. M. Carpenter. 1997. Studies of the mechanism of the periodic acid-Schiff histochemical reaction for glycogen using infrared spectroscopy and model chemical compounds. *Stain Technol.* 52: 63–77.
20. Jember, A. G., R. Zuberi, F. T. Liu, and M. Croft. 2001. Development of allergic inflammation in a murine asthma model is dependent on the costimulatory receptor OX40. *J. Exp. Med.* 193: 387–392.
21. Luna, L. C. 1968. *Manual of Histologic Staining Methods of the Armed Forces Institute of Pathology*. 3rd Ed. McGraw-Hill, New York. p. 111.
22. Rieder, G., R. A. Hatz, A. P. Moran, A. Walz, M. Stolte, and G. Enders. 1997. Role of adherence in interleukin-8 induction in *Helicobacter pylori*-associated gastritis. *Infect. Immun.* 65: 3622–3630.
23. Nakayama, J., H. Tahara, E. Tahara, M. Saito, K. Ito, H. Nakamura, T. Nakanishi, E. Tahara, T. Ide, and F. Ishikawa. 1998. Telomerase activation by hTRT in human normal fibroblasts and hepatocellular carcinomas. *Nat. Genet.* 18: 65–68.
24. Bièche, I., I. Laurendeau, S. Tozlu, M. Olivi, D. Vidaud, R. Lidereau, and M. Vidaud. 1999. Quantitation of *MYC* gene expression in sporadic breast tumors with a real-time reverse transcription-PCR assay. *Cancer Res.* 59: 2759–2765.
25. Rickles, R. J., A. L. Darrow, and S. Strickland. 1988. Molecular cloning of complementary DNA to mouse tissue plasminogen activator mRNA and its expression during F9 teratocarcinoma cell differentiation. *J. Biol. Chem.* 263: 1563–1569.
26. Belin, D., J. D. Vassalli, C. Combepine, F. Godeau, Y. Nagamine, E. Reich, H. P. Kocher, and R. M. Duvoisin. 1985. Cloning, nucleotide sequencing and expression of cDNAs encoding mouse urokinase-type plasminogen activator. *Eur. J. Biochem.* 148: 225–232.
27. Prendergast, G. C., L. E. Diamond, D. Dahl, and M. D. Cole. 1990. The c-*myc*-regulated gene *mrl* encodes plasminogen activator inhibitor 1. *Mol. Cell. Biol.* 10: 1265–1269.
28. Sabath, D. E., H. E. Broome, and M. B. Prystowsky. 1990. Glyceraldehyde-3-phosphate dehydrogenase mRNA is a major interleukin 2-induced transcript in a cloned T-helper lymphocyte. *Gene* 91: 185–191.
29. Madoiwa, S., T. Yamauchi, Y. Hakamata, E. Kobayashi, M. Arai, T. Sugo, J. Mimuro, and Y. Sakata. 2004. Induction of immune tolerance by neonatal intravenous injection of human factor VIII in murine hemophilia A. *J. Thromb. Haemost.* 2: 754–762.
30. Dano, K., P. A. Andreasen, J. Grondahl-Hansen, P. Kristensen, L. S. Nielsen, and L. Skriver. 1985. Plasminogen activators, tissue degradation and cancer. *Adv. Cancer Res.* 44: 139–266.
31. Sanai, A., H. Nagata, and A. Konno. 1999. Extensive interstitial collagen deposition on the basement membrane zone in allergic nasal mucosa. *Acta Otolaryngol.* 119: 473–478.
32. Boulet, L., M. Laviolette, H. Turcotte, A. Cartier, M. Dugas, J. Malo, and M. Boutet. 1997. Bronchial subepithelial fibrosis correlates with airway responsiveness to methacholine. *Chest* 112: 45–52.
33. Hattori, N., J. L. Degen, T. H. Sisson, H. Liu, B. B. Moore, R. G. Pandrangi, R. H. Simon, and A. F. Drew. Bleomycin-induced pulmonary fibrosis in fibrinogen-null mice. *J. Clin. Invest.* 106: 1341–1350.
34. Cho, S. H., S. W. Tam, S. Demissie-Sanders, S. A. Filler, and C. K. Oh. 2000. Production of plasminogen activator inhibitor-1 by human mast cells and its possible role in asthma. *J. Immunol.* 165: 3154–3161.
35. Mosmann, T. R., H. Cherwinski, M. W. Bond, M. A. Giedlin, and R. L. Coffmann. 1986. Two types of murine helper T cell clone. I. Definition according to profiles of lymphokine activities and secreted proteins. *J. Immunol.* 136: 2348–2357.
36. Sandler, N. G., M. M. Mentink-Kane, A. W. Cheever, and T. A. Wynn. 2003. Global gene expression profiles during acute pathogen-induced pulmonary inflammation reveal divergent roles for Th1 and Th2 responses in tissue repair. *J. Immunol.* 171: 3655–3667.
37. Del Prete, G., E. Maggi, P. Parronch, I. Chretien, A. Tiri, and D. Macchia. 1988. IL-4 is an essential factor for the IgE synthesis induced in vitro by human T cell clones and their supernatants. *J. Immunol.* 140: 4193–4198.
38. Ueda, A., N. Chandswang, and Z. Ovary. 1990. The action of interleukin-4 on antigen-specific IgG1 and IgE production by interaction in vivo primed B cells and carrier-specific cloned Th2 cells. *Cell. Immunol.* 128: 31–40.
39. Lopez, A. F., C. J. Sanderson, J. R. Gamble, H. D. Campbell, I. G. Young, and M. A. Vadas. 1988. Recombinant human interleukin 5 is a selective activator of human eosinophil function. *J. Exp. Med.* 167: 219–224.
40. Yamaguchi, Y., Y. Hayashi, Y. Sugama, Y. Miura, T. Kasahara, S. Kitamura, M. Torisu, S. Mita, and A. Tominaga. 1988. Highly purified murine interleukin 5 (IL-5) stimulates eosinophil function and prolongs in vitro survival: IL-5 as an eosinophil chemotactic factor. *J. Exp. Med.* 167: 1737–1742.
41. Gyetko, M. R., S. Sud, G. H. Chen, J. A. Fuller, S. W. Chensue, and G. B. Toews. 2002. Urokinase-type plasminogen activator is required for the generation of a type 1 immune response to pulmonary *Cryptococcus neoformans* infection. *J. Immunol.* 168: 801–809.
42. Gyetko, M. R., S. Sud, and S. W. Chensue. 2004. Urokinase-deficient mice fail to generate a type 2 immune response following schistosomal antigen challenge. *Infect. Immun.* 72: 461–467.
43. Deng, G., S. A. Curriden, G. Hu, R. P. Czekay, and D. J. Loskutoff. 2001. Plasminogen activator inhibitor-1 regulates cell adhesion by binding to the somatomedin B domain of vitronectin. *J. Cell. Physiol.* 189: 23–33.
44. Tarui, T., N. Andronicos, R. P. Czekay, A. P. Mazar, K. Bdeir, G. C. Parry, A. Kuo, D. J. Loskutoff, D. B. Cines, and Y. Takada. 2003. Critical role of integrin $\alpha_5\beta_1$ in urokinase (uPA)/urokinase receptor (uPAR, CD87) signaling. *J. Biol. Chem.* 278: 29863–29872.
45. Dawson, S. J., B. Wiman, A. Hamsten, F. Green, S. Humphries, and A. M. Henney. 1993. The two allele sequences of a common polymorphism in the promotor of the plasminogen activator inhibitor-1 (PAI-1) gene respond differently to interleukin-1 in HepG2 cells. *J. Biol. Chem.* 268: 10739–10745.
46. Eriksson, P., B. Kallin, F. M. van't Hooft, P. Bavenholm, and A. Hamsten. 1995. Allele-specific increase in basal transcription of the plasminogen activator inhibitor 1 gene is associated with myocardial infarction. *Proc. Natl. Acad. Sci. USA* 92: 1851–1855.
47. Hermans, P. W., M. L. Hibberd, R. Booy, O. Daramola, J. A. Hazelzet, and R. de Groot. 1999. 4G/5G promoter polymorphism in the plasminogen activator inhibitor-1 gene and outcome of meningococcal disease: Meningococcal Research Group. *Lancet* 354: 556–560.
48. Hellings, P. W., E. M. Hessel, J. J. van den Oord, A. Kasran, P. van Hecke, and J. L. Ceuppens. Eosinophilic rhinitis accompanies the development of lower airway inflammation and hyper-reactivity in sensitized mice exposed to aerosolized allergen. *Clin. Exp. Allergy* 31: 782–790.

JOURNAL OF VIROLOGY, Feb. 2006, p. 1874–1885 Vol. 80, No. 4
0022-538X/06/$08.00+0 doi:10.1128/JVI.80.4.1874–1885.2006
Copyright © 2006, American Society for Microbiology. All Rights Reserved.

Scalable Generation of High-Titer Recombinant Adeno-Associated Virus Type 5 in Insect Cells

Masashi Urabe,[1]* Takayo Nakakura,[1] Ke-Qin Xin,[2] Yoko Obara,[1] Hiroaki Mizukami,[1] Akihiro Kume,[1] Robert M. Kotin,[3] and Keiya Ozawa[1]

Division of Genetic Therapeutics, Jichi Medical School, Tochigi 329-0498, Japan[1]*; Department of Molecular Biodefense Research, Yokohama City University Graduate School of Medicine, Yokohama 236-0004, Japan*[2]*; and Laboratory of Biochemical Genetics, National Heart, Lung, and Blood Institute, National Institutes of Health, Bethesda, Maryland*[3]

Received 14 June 2005/Accepted 27 November 2005

We established a method for production of recombinant adeno-associated virus type 5 (rAAV5) in insect cells by use of baculovirus expression vectors. One baculovirus harbors a transgene between the inverted terminal repeat sequences of type 5, and the second expresses Rep78 and Rep52. Interestingly, the replacement of type 5 Rep52 with type 1 Rep52 generated four times more rAAV5 particles. We replaced the N-terminal portion of type 5 VP1 with the equivalent portion of type 2 to generate infectious AAV5 particles. The rAAV5 with the modified VP1 required α2-3 sialic acid for transduction, as revealed by a competition experiment with an analog of α2-3 sialic acid. rAAV5-GFP/Neo with a 4.4-kb vector genome produced in HEK293 cells or Sf9 cells transduced COS cells with similar efficiencies. Surprisingly, Sf9-produced humanized *Renilla* green fluorescent protein (hGFP) vector with a 2.4-kb vector genome induced stronger GFP expression than the 293-produced one. Transduction of murine skeletal muscles with Sf9-generated rAAV5 with a 3.4-kb vector genome carrying a human secreted alkaline phosphatase (SEAP) expression cassette induced levels of SEAP more than 30 times higher than those for 293-produced vector 1 week after injection. Analysis of virion DNA revealed that in addition to a 2.4- or 3.4-kb single-stranded vector genome, Sf9-rAAV5 had more-abundant forms of approximately 4.7 kb, which appeared to correspond to the monomer duplex form of hGFP vector or truncated monomer duplex SEAP vector DNA. These results indicated that rAAV5 can be generated in insect cells, although the difference in incorporated virion DNA may induce different expression patterns of the transgene.

Recombinant adeno-associated virus (rAAV) is being developed as a gene transfer vector. rAAV based on serotype 2 (rAAV2) successfully transduces nondividing cells, including muscle, liver, and brain cells (29). Conventional rAAV production requires packaging of rAAV DNA into type 2 capsids by transient transfection of HEK293 cells with two or three plasmids: an AAV helper plasmid encoding *rep* and *cap* genes devoid of inverted terminal repeat (ITR) sequences, a vector plasmid harboring the therapeutic gene between ITRs, and an adenovirus helper plasmid expressing E2A, virus-associated (VA) RNA, and E4orf6. Transient cotransfection is the major limitation for scale-up of rAAV production. Since rAAV can be purified using column chromatography, which can result in highly purified rAAV while eliminating other contaminating viruses, some efforts were made to develop rAAV production systems by using recombinant mammalian viruses such as adenovirus (10) or herpes virus (4) which do not rely on the plasmid transfection and therefore may be amenable to scale-up production.

Recombinant baculoviruses based on the *Autographa californica* nuclear polyhedrosis virus are widely employed for production of heterologous proteins in cultured insect cells. The highly active, late *A. californica* nuclear polyhedrosis virus promoters, such as polyhedrin and p10 promoters, regulate the expression of heterologous proteins, resulting in large amounts of foreign proteins. Insect cells may be grown in suspension cultures in volumes ranging from shake flasks of sizes from, e.g., 50 to 400 ml, up to commercial-size bioreactors, e.g., 1,000 liters and larger. Recently, we described a highly scalable and efficient method for packaging rAAV2 in insect cells by use of baculovirus expression vectors (31). The ease of scale-up production is perhaps the most attractive feature of this production system. Infection of insect cells in suspension culture with recombinant baculoviruses eliminates the transfection process. Standard downstream processing to recover rAAV, such as tangential flow filtration and column chromatography, is readily applied.

In addition to vectors derived from serotype 2, other serotypes, utilizing different cell surface receptors, constitute a vector set from which an appropriate vector can be selected for a specific application. AAV5 is the most divergent dependovirus characterized (2), and type 5 AAV vectors have desirable properties that differ from other serotype vectors. AAV5 utilizes different receptors from other serotypes (14, 30), and rAAV5 has demonstrated different tropism from AAV2 (5), thus making it worthwhile to establish a method to produce rAAV5 in insect cells.

AAV is a member of the family *Parvoviridae*. The genome of AAV is a linear, single-stranded DNA of 4.7 kb in length. The ITRs flank the unique coding sequences for the nonstructural replication initiator proteins, Rep, and the structural capsid proteins, VP. The ITRs serve as origins of DNA replication and may also function as the packaging signal. Type 2 Rep78 is generated by the p5 promoter, while Rep68 is translated from spliced mRNA from the p5 promoter. The small Rep polypep-

* Corresponding author. Mailing address: Division of Genetic Therapeutics, Jichi Medical School, 3311-1 Yakushiji, Minami-kawachi, Tochigi 329-0498, Japan. Phone: 81-285-58-7402. Fax: 81-285-44-8675. E-mail: murabe@jichi.ac.jp.

tides Rep52 and Rep40 are expressed by the p19 promoter with nonspliced or spliced mRNA. The p40 promoter regulates expression of capsid proteins VP1, VP2, and VP3. Alternate usage of two splice sites and translation of VP2 at a non-AUG codon results in a stoichiometry of 1:1:10 of VP1, VP2, and VP3. Both p5 proteins Rep78 and Rep68 are AAV origin binding proteins, and the presence of either is required for AAV DNA replication and processing replicative intermediates of the virus DNA (13). Also, either Rep52 or Rep40 is necessary for packaging the single-stranded, linear virion genome into preformed empty capsids (17). The transcriptional map of type 5 AAV differs from that of type 2; the p7 promoter or p19 promoter transcribes mRNA for Rep78 or Rep52. Type 5 AAV does not encode the spliced form of Rep polypeptides Rep68 and Rep40 (25). Structural protein VP1 is a minor constituent in the AAV capsid. But the VP1-unique portion of approximately 140 amino acid residues is highly conserved among different serotypes and has a phospholipase A_2 motif. The YXGGX and HDXXY motifs (where X is any amino acid residue) in phospholipase A_2 indicate the catalytic site and Ca^{2+} binding loop, respectively (see Fig. 3A). Enzymes classified into the secretory phospholipase A_2 family hydrolyze the ester bond at the 2-acyl ester position of glycerophospholipids in the presence of Ca^{2+} and are involved in many aspects of cellular pathways, such as lipid membrane metabolism and signal transduction pathways (1, 21). The VP1-unique portion of parvovirus is required for transfer of the virus from late endosomes to the nucleus (36). A mutant virus lacking the VP1-unique portion or the activity of phospholipase is not processed properly, and thus no virus or vector genes are expressed.

In the present study, we describe a rAAV5 production system based on recombinant baculovirus and insect cells. In order to achieve high production levels of rAAV5 particles, we replaced a portion of the VP1 polypeptide with the corresponding portion of type 2. The VP1 substitution did not alter the tropism of rAAV5, which behaved indistinguishably from rAAV5 with wild-type VP1. In an attempt to improve the yields of rAAV5 particles, we used type 1 Rep52 instead of type 5, which resulted in the production of more than 5×10^4 vector genomes (vg) per insect cell.

MATERIALS AND METHODS

Plasmid construction. A flow chart of plasmid construction is shown in Fig. 1. pSR485 is an AAV5 vector plasmid harboring green fluorescent protein (GFP) and neomycin (Neo) genes between the ITRs (27). NotI sites were introduced outside the GFP/Neo expression cassette by PCR amplification using primers 5′-GATCGTCGACGCGGCCGCTCTCAGTACAATCTGCTCTGATGCC and 5′-AGTCGTCGACGCGGCCGCCTGCAGGCATGCAAGCTTGTGAAAAA AATGC. The NotI sites (underlined) were introduced. The resulting 4-kb DNA fragment was inserted into the BglII-SalI (blunt) sites of pSR485 (pSR485n). pFB5GFP was constructed by insertion of the 4.8-kb PagI fragment from pSR485 into the Eco105III site of pFBHTΔ, which was derived from pFBHTb (Invitrogen, Carlsbad, CA) after removal of the polyhedrin promoter with BstZ17I and HindIII digestion. A humanized *Renilla* GFP (hGFP) gene was excised from phrGFPII-1 (Stratagene, La Jolla, CA) by treatment with BamHI and EcoRV and subcloned into an expression plasmid regulated by the cytomegalovirus (CMV) immediate-early promoter (pCMV). The resulting plasmid, pCMVh GFP, was treated with NotI to cut out the entire hGFP expression cassette, which was inserted into the corresponding site of pSR485n or pFB5GFP (pSR485hGFP or pFB5hGFP, respectively). A human secreted alkaline phosphatase (SEAP) gene was excised from pSEAP2-Basic (Clontech, Mountain View, CA) with NruI and SalI, and the resulting 1.8-kb fragment was blunt-ended and inserted into pCMV. The entire SEAP cassette was then excised with NotI and inserted into the corresponding site of pAAVGFP or pFBGFPR (31) between the type 2 ITRs (pAAVSEAP or pFBSEAP, respectively). The type 5 p5 Rep open reading frame (ORF) equivalent to type 2 Rep78 was PCR amplified from pAAV5-2 (2) by using primers 5′-GAAGAAGCGCGCGTATGAGTTCT CGCGAGACTTC and 5′-CGATTTACTGTTCTTTATTGGCATCGTCAA AATC and inserted into a cloning vector. The Rep ORF was cut out by NruI and BssHII, blunt-ended, and subcloned into the NotI site (blunt) of pBACΔIERep (31), which was then treated with BglII and ClaI and blunt-ended, and the resulting 2.1-kb fragment was inserted into the NotI-PstI (blunt) sites of pFBDΔ (pFBD5LR). pFBDΔ is a derivative of FastBac Dual (Invitrogen) generated by the removal of the polyhedrin and p10 promoters with NcoI and BamHI treatment. The small Rep ORF was cut out from pFBD5LR by partial digestion with Eco47III and SalI, and the resulting 1.3-kb fragment was blunt-ended and inserted into the StuI site of pFastBac Dual (pFBD5SR). pFBD5SR was then digested with BstZ17I and SalI and treated with T4 DNA polymerase, and the resulting 1.4-kb fragment was inserted into the KpnI site (blunt) of pFBD5LR (pFBD5LSR). To generate the truncated p10 promoter, complementary 5′-phosphorylated oligonucleotides 5′-TAAAATCGCGAC and 5′-CATGGTCGC GATTTTAAT were annealed to each other and inserted into the PacI-NcoI sites of pFastBac Dual (pΔ5FBD). The type 5 Rep78 gene was PCR amplified with primers 5′-GCGCTTAATTAAAATCGCTAGTATGGCTACCTTCTATGA AGTCATT-3′ and 5′-GATCGCTAGCTTACTGTTCTTTATTGGCATCGT CA-3′ and subsequently digested with PacI and NheI and inserted into the PacI-NheI sites of pΔ5FBD (pFBD5LR12) (the Rep78 ORF is capitalized). The type 5 Rep52 gene amplified using primers 5′-GATCGCGCGCCATGGCGCTCG TCAACTGGCTCGTGGAG-3′ and 5′-GATCGTCGACTTACTGTTCTTTAT TGGCATCGTCA-3′ was digested with BssHII and SalI and inserted into the corresponding sites of pFBD5LR12 (pFBD5LSR12n). To replace type 5 Rep52 on pFBD5LSR12n with type 1, 2, 3, or 4 Rep52, PCR was conducted with sense primer 5′-gatccccATGGAGCTGGTCGGGTGGCTGGTGGA-3′ and antisense primer 5′-gatcactagtTTATTGCTCAGAAACACAGTCATCCA-3′ (for type 1 or 3) or 5′-gatcactagtTTATTGTTCCATGTCACAGTCATCCA-3′ (for type 4) from AAV1 (purchased from American Type Culture Collection), an AAV2 helper plasmid pHLP19 (20), p3-2 (22), or p4-2 (3) (NcoI and SpeI sites are underlined). The resulting 1.2-kb DNA was digested with NcoI and SpeI and inserted into the corresponding sites of pFBD5LSR12n (pFBD5LSR121, pFBD5LSR122, pFBD5LSR123, and pFBD5LSR124). The resulting recombinant baculoviruses expressing type 5 Rep78 and type 1, 2, 3, 4, or 5 Rep52 are designated Rep5-1, 5/2, 5/3, 5/4, and 5/5, respectively. The type 5 VP ORF was obtained by PCR amplification from pAAV5-2 by using primers 5′-gtcaagcttcct gttaagACGTCTTTTGTTGATCACCCTCCAGATTGGT-3′ and 5′-ggatctagaTT AAAGGGGTCGGGTAAGGTATCG-3′. The sequence corresponding to the VP ORF is capitalized, and the initiation codon was mutated to ACG to reduce its translational efficiency. The 2.2-kb PCR product was cloned into pCMV (pCMV5VPm). The plasmid was digested with Acc65I and treated with T4 DNA polymerase and subsequently with XbaI to excise the VP ORF, which was then inserted into the BamHI (blunt)-XbaI sites of pFastBac Dual (pFBD5VPm). Plasmid expressing a chimeric VP was constructed by the use of an overlapping-PCR method as follows. VP251 was generated by PCR from pAAV5-2 using primers #30 and #31 (Table 1). The resulting PCR product was treated with BamHI and HindIII and cloned into the corresponding sites of pFBD5VPm. For VP252 construction, the type 2 VP portion was PCR amplified with primers #32 and #34 from pHLP19. The type 5 VP was amplified with primers #33 and #31. After gel purification, the two PCR products were combined and subjected to the second round of PCR using primers #31 and #32. Chimeric VP253, -254, -255, and -256 were produced in the same way except for primers for the first round of PCR. For VP253, primers #32 and #36 were used to amplify the type 2 VP1 portion and #31 and #35 to amplify the type 5 VP portion (see Fig. 3A). A PCR-generated chimeric VP1 gene was digested with HindIII and BamHI and inserted into the HindIII-BamHI sites of pFBD5VPm.

Cell culture. HEK293 cells were maintained in Dulbecco's modified Eagle's medium–F-12 (1:1, vol/vol, Invitrogen) supplemented with 10% fetal calf serum (Sigma-Aldrich, St. Louis, MO). *Spodoptera frugiperda* Sf9 cells (Invitrogen) were grown at 27°C in shake flask cultures containing Sf-900 II SFM (Invitrogen) supplemented with 10% fetal calf serum.

Western blotting and silver staining. Cells were lysed in 1× sodium dodecyl sulfate sample buffer and resolved on a 4 to 12% NuPAGE Bis-Tris gel (Invitrogen). After electrophoresis, separated proteins were transferred to a Durapore membrane filter (Millipore, Bedford, MA) and incubated with a primary antibody, either an anti-Rep monoclonal antibody (303.9; Research Diagnostics, Flanders, NJ) at a dilution of 1:200 or a polyclonal anti-type 5 VP antibody raised against a portion of type 5 VP3 polypeptide at a dilution of 1:50,000. The blots

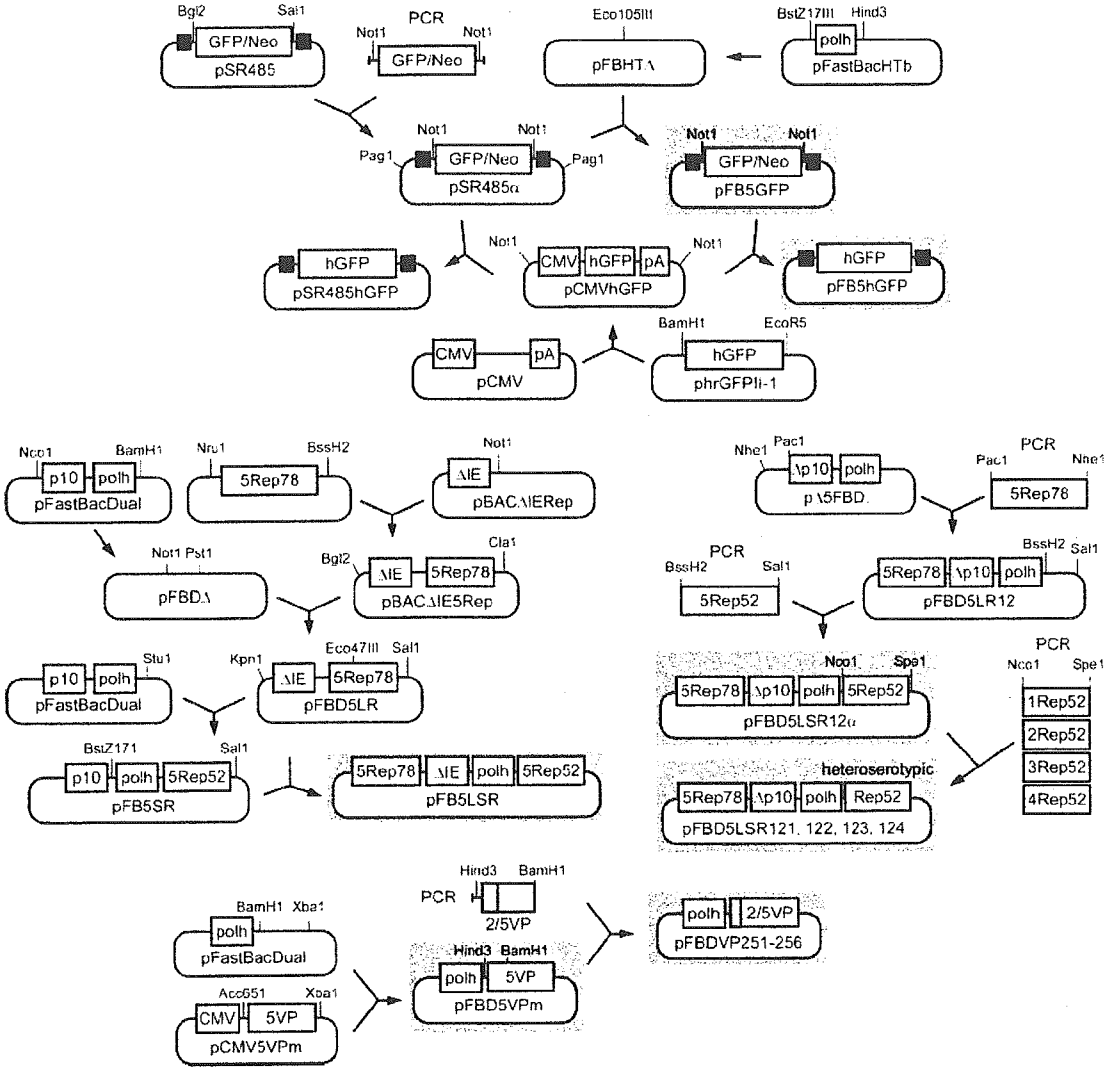

FIG. 1. Flow chart of plasmid construction. See Materials and Methods for details. Plasmids on gray backgrounds were used for generation of recombinant baculovirus vectors. Black boxes, type 5 ITR sequence; p10, p10 promoter; polh, polyhedrin promoter; pA, simian virus 40 polyadenylation sequence.

were then incubated with a secondary anti-mouse or anti-rabbit immunoglobulin G labeled with horseradish peroxidase at a dilution of 1:7,500 (Pierce, Milwaukee, WI). Membranes were incubated in Tris-buffered saline with Tween 20 (TBS-T) (10 mM Tris-HCl [pH 7.6], 0.15 M NaCl, 0.05% Tween 20, 5% nonfat dry milk). Antibodies were added to TBS-T for 1 h. After incubation, membranes were washed three times for 10 min each in TBS-T. All steps were performed at ambient temperature. The development of chemiluminescence catalyzed by horseradish peroxidase was performed according to the manufacturer's instructions (SuperSignal West Pico chemiluminescent substrate; Pierce), and the signals were detected with an X-ray film. Silver staining was performed using a SilverQuest silver staining kit (Invitrogen) according to the manufacturer's instructions.

Analysis of replicated rAAV DNA in Sf9 cells. Sf9 cells (2×10^5 cells per well) in 12-well plates were infected with GFP with or without Rep baculoviruses at a multiplicity of infection (MOI) of 3 and incubated at 27°C for 3 days. After incubation, extrachromosomal DNA was isolated by the method of Hirt (12) and a volume corresponding to 2×10^4 cells was resolved on a 0.8% agarose gel in Tris-borate buffer. Ethidium-stained gel was visualized under UV.

Production of rAAV5 in HEK293 cells. To produce rAAV5-GFP in mammalian cells, HEK293 cells at 80% confluence (approximately 10^5 cells per cm^2) in a 225-cm^2 flask were cotransfected with 27 μg of an AAV vector plasmid and 53 μg pSR487 by the calcium phosphate coprecipitation method. pSR487 harbors type 5 *rep* and *cap* genes and adenovirus E2A, E4orf6, and VA genes (27). Two days after transfection, rAAV5 was purified as described below. For production of pseudotyped type 5 rAAV-SEAP, HEK293 cells were cotransfected with pAAVSEAP; a Rep plasmid expressing type 2 Rep78, Rep68, Rep52, and Rep40; a VP plasmid expressing VP254; and an adenovirus helper plasmid.

Production and purification of rAAV5 in Sf9 cells. Typically, 4×10^8 Sf9 cells (2×10^6 cells per ml) were infected with a Rep baculovirus (RepBac), a VP baculovirus (VPBac), and a GFP baculovirus (GFPBac) with an MOI of 1 per baculovirus construct. To generate pseudotyped 2/5 rAAV-SEAP, Sf9 cells were infected with a RepBac expressing type 2 Rep78 and Rep52, VP254Bac, and SEAPBac. Pseudotype virus refers to the ITRs of one serotype packaged into a capsid derived from a different AAV serotype. For example, rAAV2/5 consists of AAV2 ITRs packaged into an AAV5 capsid. Three days after infection, the cells were pelleted by centrifugation and lysed in a lysis buffer of 20 mM Tris-HCl (pH 8.4), 50 mM NaCl, 2 mM $MgCl_2$, 0.4% deoxycholic acid, 0.5% 3-[(cholamidopropyl)-dimethylammonio]-1-propanesulfonate (CHAPS) (Merck, Darmstadt, Germany), and 60 U per ml of Benzonase (Merck) and incubated at 37°C for 30 min. The concentration of NaCl in the cell lysate was adjusted to 150 mM and incubated for an additional 30 min. Solid CsCl was added to obtain a final density of 1.36 g/cm^3. After centrifugation at 36,000 rpm for 24 h at 21°C using an SW40 Ti rotor (Beckman, Fullerton, CA), fractions containing rAAV5 were recovered and subjected to a second round of CsCl ultracentrifugation. For some experi-

TABLE 1. Oligonucleotides used for construction of chimeric VP genes

Primer	Sequence[a]
#30	5'-gtcaagcttcctgttagAcGGCTGCCGAcGGTTATCTaCCcGA TTGGTTGGAAGAAGTTGGTGAAGGT-3'
#31	5'-GCTGGGATCCGCTGGGTCCAGCTTCGGCGT-3'
#32	5'-gtcaagcttcctgttagAcGGCTGCCGAcGGTTATCTaCCcGA TTGGTTGGAGGAC-3'
#33	5'-ACAGCAGGGGTCTTGTGCTGCCTGGTTATAACTA-3'
#34	5'-TAGTTATAACCAGGCAGCACAAGACCCCTGCTGT-3'
#35	5'-GACTCGACAAGGGAGAGCCTGTCAACAGGGCAGA-3'
#36	5'-TCTGCCCTGTTGACAGGCTCTCCCTTGTCGAGTC-3'
#37	5'-GAGACAACCCGTACCTCAAGTACAACCACGCGGA-3'
#38	5'-TCCGCGTGGTTGTACTTGAGGTACGGGTTGTCTC-3'
#39	5'-GAGCAGTCTTCCAGGCGAAGAAAAGGGTTCTCGA-3'
#40	5'-TCGAGAACCCTTTTCTTCGCCTGGAAGACTGCTC-3'
#41	5'-AGGAACCTGTTAAGACGGCCCTACCGGAAAGCG-3'
#42	5'-CGCTTTCCGGTAGGGGCCGTCTTAACAGGTTCCT-3'

[a] The HindIII or BamHI sites are underlined. The initiation codon for the VP1 gene was mutated to ACG. The possible splicing donor site was destroyed by introducing silent mutations. The VP ORFs are capitalized, and mutated nucleotides are indicated by lowercase letters.

ments. rAAV5 was further purified by anion-exchange column chromatography. CsCl-banded rAAV5 fractions were dialyzed against a buffer of 20 mM Tris-HCl (pH 8.4), 20 mM NaCl, 2 mM $MgCl_2$, and 4% glycerol and loaded onto a HiTrap Q Sepharose XL column (1-ml bed volume; Amersham Biosciences, Piscataway, NJ). Bound rAAV5 was eluted with a 20 to 500 mM linear NaCl gradient. Fractions containing rAAV5 were dialyzed against a buffer of 50 mM HEPES (pH 7.4), 150 mM NaCl, 2 mM $MgCl_2$, and 5% sorbitol and stored at −80°C until use. The titer of rAAV was determined by real-time PCR with CMV-specific primers 5'-TATGGAGTTCCGCGTTACATAACTTACGGT-3' and 5'-GACTAATACGTAGATGTACTGCCAAGTAGG-3' on an HT7000 genetic analyzer (Applied Biosystems, Foster City, CA). Dilutions of pSR485 were employed as a copy number standard.

Competition experiment with a type 2 or type 5 AAV receptor analog. COS cells were plated in a 12-well plate at 30% confluence 24 h prior to infection. rAAV2-GFP or rAAV5-GFP was incubated in 0 or 20 μg per ml of heparin (Sigma-Aldrich), an analog of heparan sulfate proteoglycan (HSPG), for 2 h at room temperature. The cells were infected with adenovirus (3 PFU per cell) at 37°C for 2 h. The cells were washed with medium and then infected with rAAV2-GFP at 10^4 vg per cell or rAAV5-GFP at 10^5 vg per cell. At 24 h postinfection, the cells were visually examined under a fluorescent microscope and the percentages of positive cells were determined by flow cytometric analysis of 10^5 infected cells. Experiments were performed in triplicate. Competition experiments with α2-3 sialic acid were performed as described previously (14). COS cells were plated at 30% confluence 1 day before infection in a 12-well plate. The cells were infected with adenovirus (3 PFU per cell) and incubated at 37°C for 2 h. The adenovirus-containing medium was removed, and the cells were washed with medium. The cells were then infected with rAAV2-GFP (10^4 vg per cell) or rAAV5-GFP (10^5 vg per cell) for 1.5 h in 0 or 0.5 mM 3'-*N*-acetylneuraminyl-*N*-acetyllactosamine (3'-SLN) (Sigma-Aldrich), an analog of α2-3 sialic acid. The cells were washed twice with medium and further incubated for 1 day. The cells were then examined for GFP fluorescence, and the number of positive cells was measured by flow cytometry.

Treatment of cells with neuraminidase. COS cells were infected with adenovirus at 3 PFU per cell for 1 h at 37°C. The cells were treated with 0.08 U per ml of neuraminidase (*Vibrio cholerae*, type III; Sigma-Aldrich) for 1 h and infected with rAAV2-GFP at 10^4 vg per cell or rAAV5-GFP at 10^5 vg per cell for 2 h. The infected cells were then washed twice with medium and incubated for 1 additional day. The GFP-positive cells were counted by flow cytometry. Experiments were done in triplicate.

Muscle injection of rAAV5 in mice. A total of 10^{11} vg of pseudotyped rAAV5-SEAP produced in either 293 cells or Sf9 cells were injected into murine tibialis anterior muscles and blood was taken at the indicated weeks after injection. The serum SEAP activity was measured by a SEAP report gene assay (Roche Diagnostics, GmbH, Penzberg, Germany). The mouse study was approved by a review board at Jichi Medical School.

RESULTS

Construction of recombinant VP and Rep baculoviruses. Production of rAAV2 in insect cells uses three baculovirus vectors providing the following: (i) genes for three AAV structural proteins that form the virus capsid (VP1, VP2, and VP3), (ii) two of the AAV nonstructural proteins for replication and encapsidation (Rep78 and Rep52), and (iii) AAV vector DNA consisting of the gene of interest flanked by the AAV origins of replication (ITRs). In the presence of the AAV nonstructural proteins, the AAV vector DNA is "rescued" from the baculovirus genome and replicates as AAV via the ITRs (31).

Similarly to AAV type 2, the type 5 capsid proteins VP1, VP2, and VP3 are synthesized from two spliced mRNAs arising from the p41 promoter (Fig. 2A) (25). One mRNA is translated into VP1, while another transcript encodes VP2 and VP3. The initiation codon for VP2 is ACG, which is poorly utilized, resulting in the ribosome scanning through to the VP3 initiation codon AUG. The alternate usage of two acceptor sites and the poor utilization of the ACG initiation codon for VP2 are responsible for the 1:1:10 stoichiometry of VP1, VP2, and VP3. As shown in our previous report, the type 2 VP gene with an AAV intron does not express all of the VP polypeptides in insect cells (31). Mutating the VP1 AUG initiation codon to ACG resulted in production of VP1, VP2, and VP3 with a stoichiometry of approximately 1:1:10 from a single transcript without alternate splicing (31). Based on our initial success with AAV2, we constructed a similar type 5 VP baculovirus (VP5Bac) that harbored a type 5 VP gene where the initiation codon for VP1 was changed to ACG (Fig. 2B). Although this VP5Bac was able to produce type 5 capsids into which type 5 AAV vector DNA was incorporated, VP1 was poorly expressed compared to that synthesized in 293 cells (Fig. 2C). The resulting rAAV5-GFP particles poorly transduced COS cells. The calculated ratio of vector genomes to transducing units for the Sf9 cell-produced rAAV5-GFP was 10 times higher than the ratio for the 293 cell-produced counterpart. The VP1 polypeptides have phospholipase A_2 activity and are critical for efficient transfer of the viral genome from late endosomes to the nucleus (36). The efficiency with which a scanning eukaryotic ribosome recognizes an AUG codon for translational initiation is dependent on the local sequence context of the codon. The sequence ACC**AUG**G is optimal for initiation (18). Residue G at +4 seems particularly important for translation from a non-AUG codon where the A of the AUG codon is defined as +1 (11). In type 2 VP1, the nucleotide at +4 is G while the corresponding nucleotide at +4 in type 5 is U. To increase the efficiency of translation from an ACG codon for type 5 VP1 in insect cells, we tested some VP1 mutants that introduced a G residue at +4. However, these mutants also failed to produce infectious type 5 AAV particles (data not shown). The VP1-unique portion is conserved well among different serotypes compared to the VP3 portion that constitutes the majority of the viral capsids and is responsible for receptor binding specificity. The type 5 VP1-unique portion is approximately 70% identical to the equivalent portion of type 2 (Fig. 3A), while the type 5 VP3 portion is 60% homologous to the equivalent portion of type 2 (2). Since we successfully produced rAAV2 that was as infectious as the 293 cell-produced one, we tested a series of chimeric capsids between types 2 and 5 in which a part of the type 5 VP1-unique portion was replaced by the corresponding portion of type 2 VP1. Figure 3A shows the chimeric VP1 genes constructed. Figure 3B shows the Western analysis of type 5 VP poly-

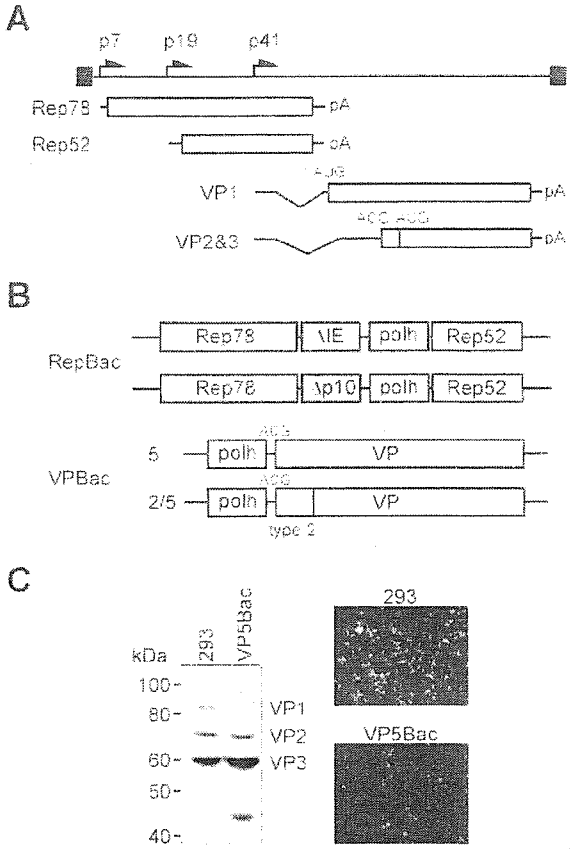

FIG. 2. (A) Genetic and transcriptional map of type 5 AAV. The p7 and p19 promoters drive Rep78 and Rep52, respectively. The p41 promoter transcribes two mRNAs. One expresses VP1, and the other is for VP2 and VP3. The initiation codon for VP2 is ACG, which is poorly utilized for translation, leading to production of a smaller amount of VP2 polypeptides than VP3 polypeptides. The ITRs are indicated by black boxes. pA, polyadenylation signal sequence. (B) Recombinant baculoviruses (rBac) constructed. An rBac for Rep utilizes a truncated promoter for the immediate-early 1 gene of *Orgyia pseudotsugata* nuclear polyhedrosis virus (ΔIE) for type 5 Rep78, and another RepBac expresses Rep78 under the control of a truncated p10 promoter (Δp10). See Fig. 4A for details. Either RepBac uses the polyhedrin promoter (polh) for Rep52. For expression of type 5 capsid proteins, a recombinant baculovirus that harbored a VP gene on which the initiation codon for VP1 is mutated to ACG was constructed (VP5Bac). Another series of VPBacs that had the type 5 VP1 gene partially replaced by the corresponding portion of type 2 VP1 at the N terminus was generated. (C) Western analysis of Sf9 cells infected with VP5Bac. The initiation codon for VP1 was mutated to an ACG codon, which enabled synthesis of VP1, -2, and -3 from a single VP mRNA. The amount of VP1 synthesized was extremely small compared to that in 293 cells. rAAV5-GFP generated with VP5Bac was used for the infection of COS cells at 10^5 vg per cell. The number of GFP-positive cells was 10% of the number of positive cells obtained with rAAV5-GFP produced in 293 cells.

peptides produced with VP251Bac through VP256Bac. Each VPBac produced chimeric VP1 at levels comparable to those of VP2. Formation of empty capsids was confirmed by CsCl density gradient analysis of Sf9 cell lysate infected with VP254Bac, as shown in Fig. 3C. The peak of VP polypeptides came to the fraction of 1.31 g/cm^3, a buoyant density of empty capsids. The GFP gene between the type 5 ITRs could be packaged into each type of chimeric capsid, and all of the chimeric rAAV5-GFPs except VP251 could transduce COS cells with efficiency similar to that of 293 cell-produced rAAV5-GFP (data not shown). The yields of rAAV5-GFP produced with VP253Bac or VP254Bac were approximately 1.2 times higher than others, although the difference was not statistically significant. We thus used VP254Bac to produce rAAV5 for the next experiments.

The initial Rep baculovirus for type 2 rAAV production drove type 2 Rep72 expression with a truncated promoter for the immediate-early 1 gene of *Orgyia pseudotsugata* nuclear polyhedrosis virus (ΔIE) and type 2 Rep52 under the control of the polyhedrin promoter (31) (Fig. 2B). The AAV5 genome encodes nonstructural proteins Rep78 and Rep52 (Fig. 2A). Similarly, we constructed a Rep baculovirus that expressed type 5 Rep78 and Rep52 under the control of the ΔIE promoter and the polyhedrin promoter, respectively. The titers of the type 2 or type 5 Rep baculoviruses, however, were lower than those of other recombinant baculovirus vectors (e.g., VPBac, GFPBac). The immediate-early 1 gene promoter becomes active at the early stage of baculovirus infection, and we thought that early expression of Rep78 in insect cells might negatively affect the yields of recombinant baculoviruses. The very late p10 promoter, which is widely used for recombinant protein production, is active at the latest stage of baculovirus infection. Thus, to delay and suppress the expression of Rep78, we tested a series of truncated p10 promoters. First, we screened the truncated p10 promoters for production of type 2 rAAV and selected one that generated high-titer rAAV2. Figure 4A shows the map of the p10 promoter and the truncated p10 promoter we constructed. The upstream TAAG sequence does not affect the activity of the p10 promoter (32). The sequence between the TAAG sequence and the p10 protein initiation codon at +72 (where the transcription start site is defined as +1) is called the burst sequence and is required for the "burst" of expression of the p10 protein at the very late stage of baculovirus infection. The *vlf-1* transactivator interacts with the burst sequence and strongly stimulates the transcription from the p10 promoter (35). To construct a weak p10 promoter (Δp10), we removed the burst sequence between positions +39 and +72 from the original p10 promoter. The Δp10 promoter was best for the production of rAAV2 among a series of truncated p10 promoters we examined. The titers of recombinant baculoviruses with the Δp10 promoter were comparable to those of other recombinant baculoviruses. The Δp10 promoter was transferred to express type 5 Rep78 (Fig. 2B). Figure 4B compares the time courses of type 5 Rep expression by ΔIE and Δp10 promoters over 72 h after infection, indicating that the Δp10 promoter-driven Rep78 expression was detected at 24 h after infection while the ΔIE promoter expressed Rep78 as early as 12 h after infection. To examine whether this modest difference in the levels of Rep78 affected replication of the AAV vector DNA, we isolated the low-molecular-weight DNA from the Sf9 cells infected with hGFP baculovirus and a Rep baculovirus (Fig. 4C). A ladder of replicative forms (RF) of rAAV5 DNA began to appear at 36 h postinfection in either case. The expected size of rAAV5-hGFP or monomer RF is 2.4 kb and the sizes of dimer and trimer RF are 4.8 and 7.2 kb, which is consistent with the result of the agarose gel electrophoresis.

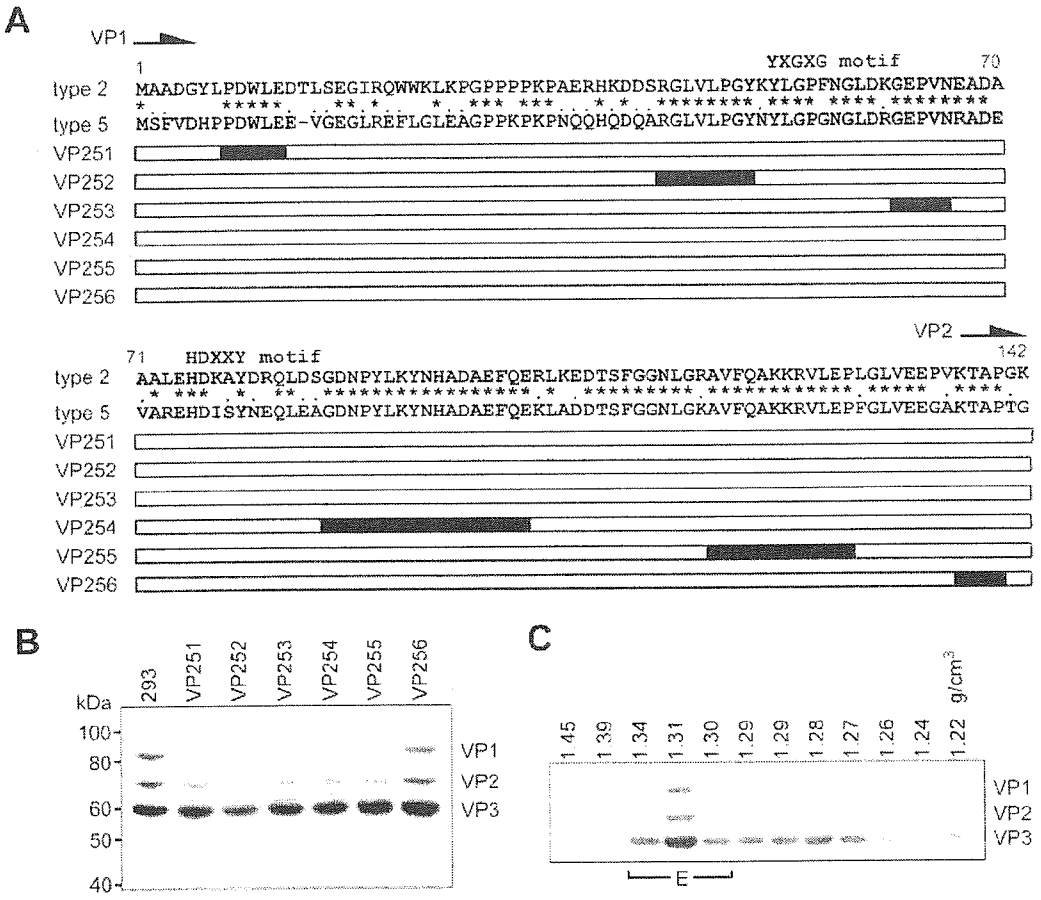

FIG. 3. (A) Chimeric VP genes constructed. The portions derived from type 2 are indicated in gray, while those from type 5 are in white. The common portions are indicated in black. The phospholipase A_2 motifs are shaded. The YXGGX and HDXXY motifs (where X is any amino acid residue), indicating the catalytic site and Ca^{2+} binding loop, respectively, are also shown. The amino acid residues common between type 2 and type 5 are indicated by asterisks. Amino acid residues classified into the same group are indicated by dots. (B) Expression of chimeric VP polypeptides in Sf9 cells. One microgram of cell lysate was resolved onto a 4 to 12% NuPAGE Bis-Tris gel in MOPS (morpholinepropanesulfonic acid) buffer (Invitrogen). Separated proteins were transferred to a Durapore membrane (Millipore), and VP proteins were detected with a rabbit polyclonal antibody raised against the type 5 VP3 portion. The lane labeled 293 shows lysate from HEK 293 cells transfected with pSR487, a hybrid plasmid harboring type 5 AAV *rep* and *cap* genes and adenovirus E2A, VA RNA, and E4orf6 genes (27). Lanes labeled VP251 through VP256 indicate lysates from Sf9 cells infected with recombinant baculovirus expressing chimeric VP. (C) Chimeric VP between types 2 and 5 is able to form empty particles. Sf9 cells (1×10^7 cells) infected with a VP2/5Bac, VP253Bac, were lysed as described in Materials and Methods. Solid CsCl was added to make a buoyant density of 1.30 g/cm^3. After ultracentrifugation for 24 h at 36,000 rpm at 21°C using an SW40 Ti rotor (Beckman), 1-ml fractionations were collected. A portion of each fraction was resolved onto a 4 to 12% NuPAGE gel in MOPS buffer, transferred to a Durapore membrane, and detected with a rabbit anti-type 5 VP polyclonal antibody. The buoyant density of each fraction is indicated above each lane. Fractions that contain empty capsids are indicated by E.

Heteroserotypic small Rep can package rAAV5 DNA into type 5 capsids. The insect cell-based production system for rAAV2 or rAAV1 can generate more than 4×10^4 particles of rAAV per Sf9 cell. However, the yields of rAAV5 produced with either ΔIE or Δp10 RepBac were approximately 1×10^4 to 2×10^4 vg per Sf9 cell. Rep52, or small Rep protein, has been implicated in encapsidation of the AAV genome (17). To establish a high-titer production system, we investigated the use of other serotypes of Rep52 for rAAV5 production. We replaced the type 5 Rep52 with serotype 1, 2, 3, or 4 Rep52 on the Δp10 RepBac. Figure 5A shows the results of Western blotting of Sf9 cells infected with Rep baculoviruses expressing type 5 Rep78 under the control of the Δp10 promoter and serotype 1, 2, 3, 4, or 5 Rep52 driven by the polyhedrin promoter. To generate rAAV5, Sf9 cells were coinfected with hGFPBac, VP254Bac, and a RepBac with the indicated serotype Rep52 at an MOI of 1. Sf9 cells infected with hGFPBac and VP254Bac along with RepBac producing type 1 Rep52 were processed by CsCl density centrifugation, and fractions were analyzed for capsid antigen by Western blotting (Fig. 5B). Two peaks of VP proteins were detected; the higher-buoyant-density peak, from 1.42 to 1.36 g/cm^3, presumably consists of a vector genome containing rAAV5 particles. Another peak, at 1.33 g/cm^3, represents empty capsids, indicating that type 1 Rep52 packaged serotype 5 rAAV DNA into type 5 capsids. When a RepBac that expressed only type 5 Rep78 was used, no rAAV5 particles were produced, confirming that heteroserotypic small Rep indeed packaged type 5 rAAV DNA into type 5 capsids. The cell lysate was loaded directly onto an anion-exchange column, and purified particles were investigated un-

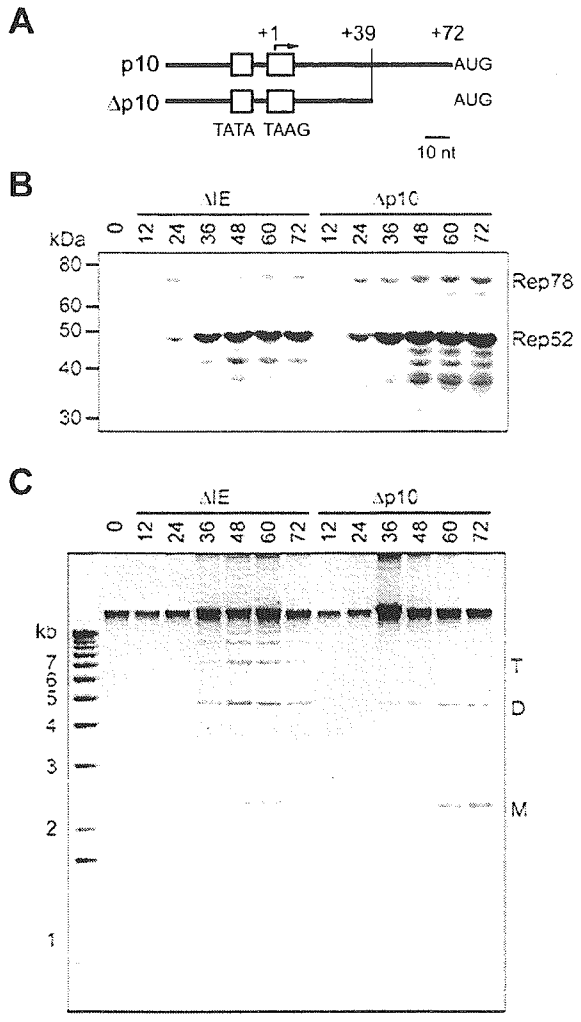

FIG. 4. (A) Map of the Δp10 promoter used for Rep78 expression. The sequence between positions +39 and +72 is deleted in the Δp10 promoter, where the T of the TAAG sequence or the transcription start site (marked with a bent arrow) is defined as +1 and the A of the p10 protein AUG codon is defined as +72. The original AUG codon for the p10 protein was mutated to ACT with pFastBac Dual (Invitrogen). The positions of the TATA box and the TAAG sequence are indicated. (B) Time course of Rep78 expression by ΔIE or Δp10 promoter. Sf9 cells were infected with a Rep baculovirus, and the cells were harvested at the times indicated (in hours) for Western analysis with a monoclonal anti-Rep antibody. (C) Replication of hGFP vector DNA in insect cells. Sf9 cells were coinfected with a Rep baculovirus and an hGFP baculovirus at 1 PFU per cell and incubated for the times indicated (in hours). Low-molecular-weight DNA was isolated, and DNA equivalent to 10^5 cells was resolved onto a 1% agarose gel. T, trimer replicative form; D, dimer; M, monomer.

der electron microscopy, showing typical rAAV particles of a diameter of 20 nm in addition to empty capsids (Fig. 5C). According to the staining pattern, approximately 30% of capsids contained vector genomes. In another experiment, rAAV5-hGFP was purified with two rounds of CsCl ultracentrifugation and the titers of rAAV5-hGFP were determined by real-time PCR using a pair of CMV-specific primers. Figure 5D summarizes the yields of rAAV5-hGFP with the use of different serotypes of small Rep. The titer of rAAV5-GFP produced with type 1, 2, 3, or 4 small Rep was 56,000 ± 3,200 (n = 4), 41,000 ± 18,900 (n = 4), 42,000 ± 7,300 (n = 3), or 39,000 ± 3,500 (n = 3) particles per Sf9 cell, respectively, while that of rAAV5-GFP produced using AAV5 Rep52 was 13,500 ± 3,200 (n = 5). The rAAV5-hGFP particles produced with the indicated serotype Rep52 were further purified by anion-exchange column chromatography, and a total of 3×10^9 vg of either rAAV5-hGFP were then fractionated by sodium dodecyl sulfate-polyacrylamide gel electrophoresis and examined by silver staining along with 293 cell-produced rAAV5-hGFP (Fig. 5E). Densitometric analysis indicated that the intensities of the VP3 bands were almost equal to one another.

Type 5 vector DNA was packaged into type 5 capsids consisting of chimeric VP1 between types 2 and 5 in the baculovirus system. To examine the possible effect of the chimeric VP1 on packaging of type 5 vector DNA with heteroserotypic Rep52, we tested the production of rAAV5-hGFP by using either Rep5/1Bac or Rep5/5Bac and VP5Bac or VP254Bac. Interestingly, the yields of rAAV5 produced with type 5 Rep52 and type 2/5 chimeric capsids were constantly lower than yields produced with other combinations (Fig. 5F). Type 1 Rep52 was capable of packaging type 5 vector DNA into type 5 capsids and type 2/5 chimeric capsids with similar levels of efficiency. Although the result was not conclusive, the presence of a type 2 VP1-unique portion might interfere with type 5 Rep52 packaging rAAV5 DNA into type 5 capsids in insect cells.

Insect cell-produced rAAV5 infects cells via an α2-3 sialic acid receptor. AAV2 capsids utilize HSPG as a primary coreceptor to infect target cells (30), whereas AAV5 capsids require α2-3 sialic acid for efficient uptake (14). rAAV5 capsids generated in Sf9 cells are composed of VP1 partially replaced with type 2 VP1. The domains involved in receptor binding are within the VP3 portion (16), and the type 2 VP1-unique portion does not appear to be involved in attachment to target cells (19). To determine whether rAAV5 chimeric capsid particles infect cells via sialic acid and not via HSPG, we performed competition experiments with receptor analogs. The results of the heparin competition study show that rAAV2-GFP failed to transduce COS cells in the presence of heparin, an analog of heparan sulfate, as expected (Fig. 6A, top panels). By contrast, rAAV5-GFP produced in 293 cells (Fig. 6A, middle panels) or insect cells (Fig. 6A, bottom panels) was able to express GFP in COS cells irrespective of the presence of heparin, suggesting that Sf9 cell-produced rAAV5-GFP did not utilize HSPG as a primary coreceptor. The number of GFP-expressing cells was counted by flow cytometry, and the percent change in transduction compared to transduction in the absence of heparin was calculated, which clearly corroborated the observation with fluorescent microscopy. We next examined whether insect cell-produced rAAV5-GFP infects cells via α2-3 sialic acid. As shown in Fig. 6B, COS cells were infected with rAAV5 generated in 293 cells (middle panels) or Sf9 cells (bottom panels) in the presence or absence of an analog of α2-3 sialic acid, 3′-SLN. The analog inhibited GFP expression in COS cells by both 293 cell- and Sf9 cell-produced rAAV5-GFP, suggesting that rAAV5-GFP produced in insect cells infected cells via α2-3 sialic acid as did 293 cell-produced rAAV5. To confirm that rAAV5-GFP derived from insect cells utilized sialic acid as a cell attachment receptor, we infected cells denuded of sialic acid by neuraminidase treatment. The

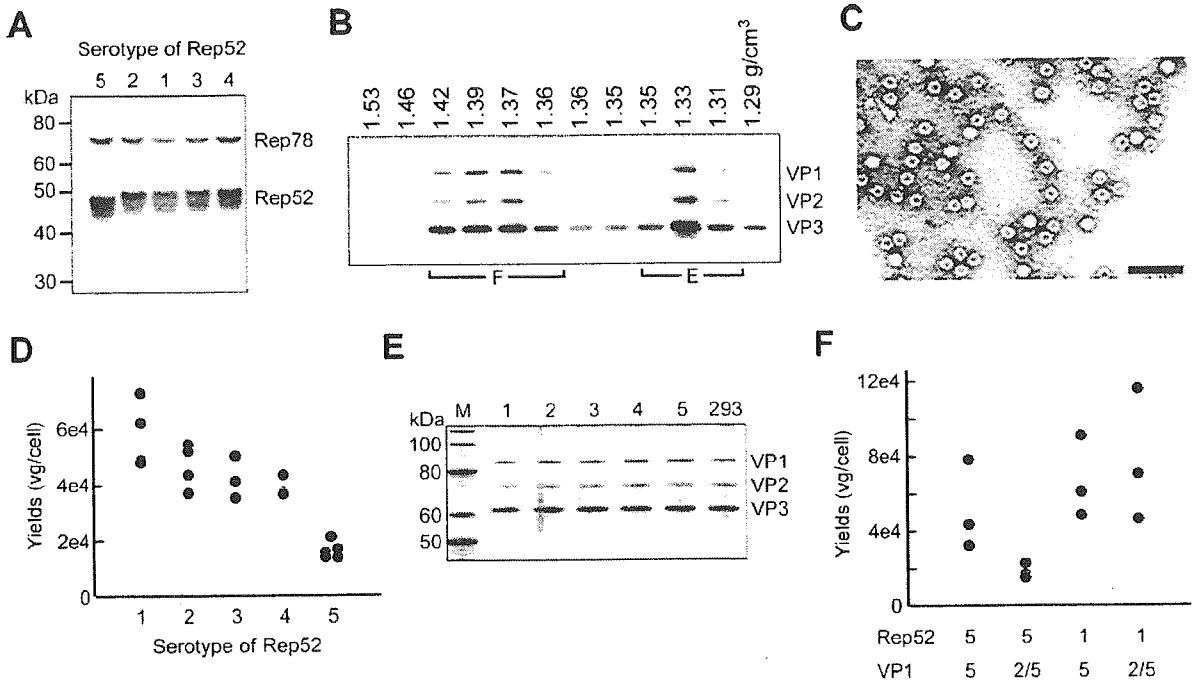

FIG. 5. (A) Western analysis of RepBacs expressing type 5 Rep78 and type 1, 2, 3, 4, or 5 Rep52 with an anti-Rep antibody. (B) Analysis of Sf9 cells coinfected with Rep, VP254, and hGFP baculoviruses by CsCl density gradient ultracentrifugation. Three days after infection, the cells were lysed and subjected to ultracentrifugation. F, filled, or containing rAAV particles; E, empty capsids. (C) Negative staining of rAAV5-hGFP particles purified with ion-exchange column chromatography alone. Particles were stained with 2% uranyl acetate. Magnification, ×100,000. Bar, 100 nm. (D) Generation of rAAV5-hGFP produced with different serotypes of Rep52. The yield of rAAV5-GFP produced with type 1, 2, 3, 4, or 5 small Rep was 56,000 ± 3,200 (n = 4), 41,000 ± 18,900 (n = 4), 42,000 ± 7,300 (n = 3), 39,000 ± 3,500 (n = 3), or 13,500 ± 3,200 (n = 5) particles per Sf9 cell, respectively. (E) Analysis of rAAV5-hGFP produced in insect cells or 293 cells by silver staining. rAAV5-hGFP (3×10^9 particles) produced with serotype 1, 2, 3, 4, or 5 and that produced in 293 cells were resolved onto a 4 to 12% NuPAGE Bis-Tris gel (Invitrogen). Lane M, molecular size markers. (F) Comparison of the yields of rAAV5-GFP produced with type 1 or type 5 Rep52 and VP5Bac or VP2/5Bac. Sf9 cells were coinfected with hGFPBac, Rep5/1Bac or Rep5/5Bac, and VP5Bac or VP254Bac at an MOI of 1 in each of three independent experiments. The rAAV5-hGFP produced was purified by two rounds of CsCl density gradient ultracentrifugation, and the genomic titer was determined by real-time PCR.

result shows that prior incubation with neuraminidase significantly inhibited the transduction of COS cells mediated by rAAV5-GFP produced in 293 cells and Sf9 cells (Fig. 6C).

Comparison of transduction efficiencies with rAAV5 in cultured cells. We next compared the efficacy of rAAV5-GFP/Neo produced in Sf9 cells to that for a mammalian-cell-produced counterpart. COS cells were infected with either Sf9-produced or 293-produced rAAV5-GFP/Neo at 1×10^5 through 1×10^2 vg per cell for 1 day, and the number of GFP-positive cells was counted by flow cytometry. As shown in Fig. 7A, both Sf9-produced and 293-produced rAAV5-GFP/Neo showed similar dose-response curves. In addition, the vector genome-to-transducing unit ratio was calculated based on the number of GFP-positive cells at 3×10^3 vg per cells. Three independently produced samples were examined, and the vector genome-to-transducing unit ratio for Sf9-produced rAAV5-GFP was $3.9 \times 10^4 \pm 1.6 \times 10^4$ (mean ± standard deviation), while the ratio for 293-produced rAAV was $3.6 \times 10^4 \pm 1.2 \times 10^4$. These results indicated that insect cell-generated rAAV5-GFP/Neo had a similar ability to transduce COS cells. Although the capsids produced in Sf9 cells contain type 2/5 chimeric VP1 and those produced in HEK293 cells were composed of original type 5 VP1, rAAV5-GFP/Neo derived from Sf9 cells and that derived from HEK293 cells did not show any significant difference in GFP expression in COS cells, suggesting that the difference in the VP1-unique portion did not impact the expression of the transgene or affect the intracellular processing of type 5 capsids in COS cells. We also compared transduction efficiencies of rAAV5-hGFP generated in Sf9 cells and rAAV5-hGFP generated in HEK293 cells. Surprisingly, the dose-response curve obtained by Sf9-produced rAAV5-hGFP shifted to the right and the number of GFP-positive cells at the dose of 3×10^5 vg per cell was five times larger than that for 293-produced rAAV5-hGFP (Fig. 7B). Since the substitution of the type 5 VP1-unique portion with the equivalent portion of type 2 did not impact the GFP expression in COS cells (Fig. 7A), we explored the rAAV genomes packaged into vector capsids. Virion DNA was isolated and analyzed on an alkaline gel. After electrophoresis, the DNA was transferred to a nylon membrane and hybridized with a ^{32}P-labeled CMV-specific probe. The GFP/Neo DNA packaged into AAV5 capsids is essentially the same in size and amount as expected (Fig. 7C). We next analyzed virion DNA isolated from rAAV5-hGFP produced with the indicated serotype Rep52 in insect cells, as well as 293-produced rAAV5-hGFP (Fig. 7D). The encapsidated hGFP DNA is present as

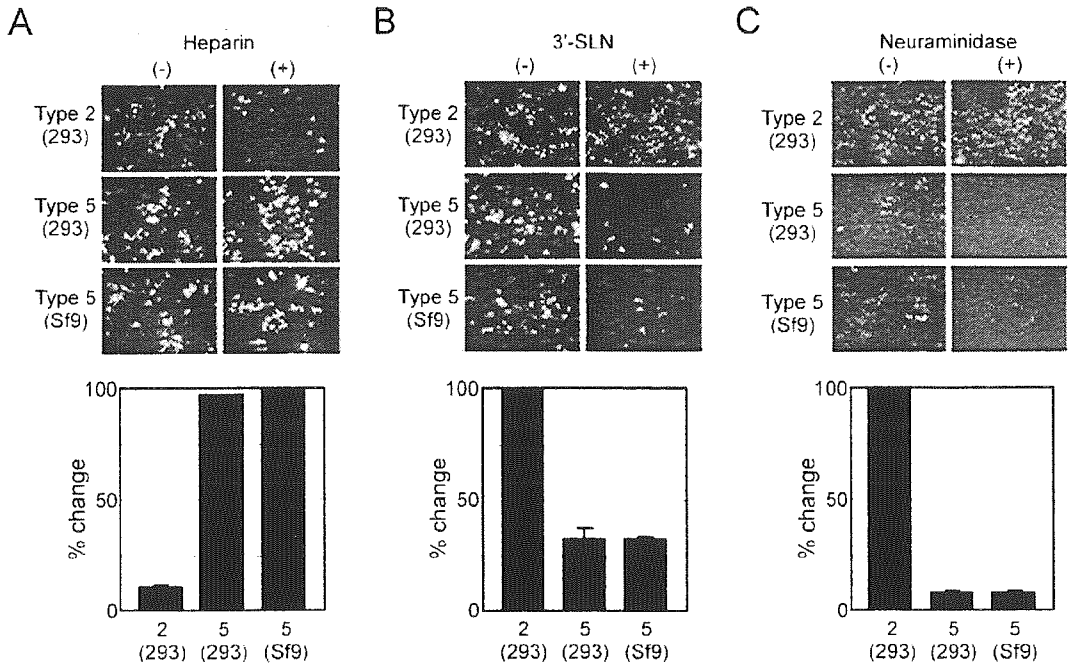

FIG. 6. (A) Heparin, an analog of HSPG, does not inhibit transduction of COS cells infected with rAAV5-GFP/Neo produced in insect cells. Cells were infected with adenovirus at 3 PFU per cell and incubated at 37°C for 2 h. After being washed with medium, the cells were infected with rAAV2-GFP/Neo produced in 293 cells at 10^4 vg per cell or rAAV5-GFP/Neo generated in 293 cells or Sf9 cells at 10^5 vg per cell in the presence or absence of 20 μg per ml of heparin in triplicate. One day after infection, the cells were observed under a fluorescent microscope. The number of GFP-positive cells was also counted by flow cytometry. Data are presented as percent change in transduction compared to transduction in the absence of heparin. (B) An analog of α2-3 sialic acid inhibits both 293 cell- and Sf9 cell-produced rAAV5-GFP/Neo. COS cells were infected with an adenovirus at 3 PFU per cell and incubated at 37°C for 2 h. After being washed with medium, the cells were infected with rAAV2-GFP/Neo at 10^4 vg per cell or rAAV5-GFP at 10^5 vg per cell for 1.5 h in the presence of 0 or 0.5 mM 3'-SLN (Sigma-Aldrich). The cells were washed twice with medium and further incubated for 1 day. The number of GFP-expressing cells was measured by flow cytometry ($n = 3$). Data are presented as percent change in transduction compared to transduction in the absence of the analog. (C) Neuraminidase treatment of COS cells inhibits transduction with rAAV5-GFP generated in 293 cells or Sf9 cells. COS cells were infected in triplicate with adenovirus at 3 PFU per cell for 1 h at 37°C, treated with 0.08 U per ml of neuraminidase (*Vibrio cholerae*, type III; Sigma-Aldrich) for 1 h, and infected with 10^5 vg per cell of rAAV5-GFP produced in 293 cells or Sf9 cells for 2 h. COS cells were similarly treated and also infected with 10^4 vg per cell of rAAV2-GFP/Neo. The infected cells were then washed twice with medium and incubated for an additional day. After incubation, the cells were observed under fluorescent microscopy and the number of GFP-positive cells was counted by flow cytometry.

two DNA species. The higher-mobility virion DNA corresponds with 2.4-kb hGFP vector DNA or a single-stranded monomer, which is confirmed by comigration with a 2.4-kb vector DNA obtained by treatment with a restriction enzyme of the hGFP vector plasmid, pSR485hGFP. The lower-mobility DNA is the same in size as the monomer RF or duplex form of hGFP DNA (Fig. 7D) isolated from Sf9 cells coinfected with RepBac and hGFPBac (Fig. 4C). The intensity of the larger virion DNA, which was quantified with an imaging analyzer, was roughly double that of shorter DNA for each rAAV5 produced in Sf9 cells. If the larger virion DNA is a monomer duplex form and thus has two CMV promoter sequences hybridizing to a CMV probe, then we estimated that the quantity of the double-stranded monomeric form was equal to that of the single-stranded monomer. The ratio of the amount of the monomer duplex form to the amount of the single-stranded monomer form in the rAAV5-hGFP virion produced in 293 cells is 1 to 3.5. AAV particles have been shown to package two copies of vector genomes that are less than 50% of the 4.8-kb AAV genome, and the packaged vector DNA appeared to be monomeric single-stranded and double-stranded RF (6). For gene expression, the single-stranded vector genome has to be converted to a double-stranded form by either second-strand synthesis (8, 9) or annealing of complementary strands (23). The monomeric duplex vector DNA, on the other hand, can function directly as a template for mRNA synthesis. Thus, the more potent gene expression mediated by rAAV5-hGFP generated in Sf9 cells is probably due to the presence of the encapsidated monomer duplex form.

Comparison of efficacies of rAAV5 in vivo. To compare the efficacies of rAAV5 produced in 293 cells and rAAV5 produced in Sf9 cells, we constructed a type 5 vector that expressed human SEAP. rAAV5 particles produced in Sf9 cells consisted of chimeric VP1 between type 2 and type 5. To eliminate the possible difference in intracellular processing of rAAV5 particles due to replacement of the type 5 VP1-unique portion with the equivalent one of type 2, we compared the in vivo activities of rAAV5 particles containing type 2/5 VP1 polypeptides produced in insect and mammalian cells. Five mice each intramuscularly received a total of 10^{11} vg of rAAV5-SEAP generated in either 293 cells or Sf9 cells, and serum SEAP levels were monitored. As shown in Fig. 8A, the expression profile of the Sf9-produced type 5 SEAP vector differed from that of the 293-produced one. The rAAV5-SEAP